Supporting Information

Nicotinamide Mononucleotide Synthetase is the key enzyme for an alternative route of NAD biosynthesis in *Francisella tularensis*

Leonardo Sorci[*], Dariusz Martynowski[†], Dmitry A. Rodionov[*], Yvonne Eyobo[†], Xhavit Zogaj[‡], Karl E. Klose[‡], Evgeni V. Nikolaev[¶], Giulio Magni[‖], Hong Zhang[†], Andrei L. Osterman[*,**,††]

[*]Burnham Institute for Medical Research, 10901 North Torrey Pines Road, La Jolla, CA 92037; [†]Department of Biochemistry, University of Texas Southwestern Medical Center, Dallas, TX 75390; [‡]South Texas Center for Emerging Infectious Diseases, University of Texas, San Antonio, TX 78249; [¶]Department of Pathology, Anatomy and Cell Biology, and Daniel Baugh Institute for Functional Genomics and Computational Biology, Thomas Jefferson University, Philadelphia, PA 19107; [‖]Istituto di Biotecnologie Biochimiche, Università Politecnica delle Marche, 60131 Ancona, Italy; [**]Fellowship for Interpretation of Genomes, Burr Ridge, IL 60527

Methods

Chemicals and strains.

Buffers, salts, and reagents, including the assay components ATP, NMN, NaMN, NAD, NaAD, ADP-ribose, inorganic pyrophosphatase and alcohol dehydrogenase were purchased from standard commercial sources. Enzymes for PCR and DNA manipulations were from New England Biolabs Inc. (Beverly, MA). Plasmid purification kits were from Promega (Madison, WI). PCR purification kits were from Roche Diagnostics (Indianapolis, IN). Nickel-nitrilotriacetic acid resin was from Qiagen Inc. (Valencia, CA). Oligonucleotides for PCR and sequencing were synthesized by Sigma-Genosys (Woodlands, TX). *E. coli* strains DH5α (Invitrogen) and BL21/DE3 (Stratagene, La Jolla, CA) were used for gene cloning and protein overexpression, respectively.

Gene cloning, protein overexpression and purification

Generation of *F. tularensis* and *B. anthracis* expression constructs. The genes for *ft*NadE* and *ft*NadM (locus tags FTL_0685 and FTL_0452, respectively) were amplified by PCR from *F. tularensis* subsp. Holarctica LVS genomic DNA. The genes for *ba*NadD and *ba*NadE (BA_1998 and BA_4558, respectively) were PCR-amplified from *B. anthracis* strain Ames genomic DNA (gifted by Dr. R. Liddington). The following primers were used:
*ft*NadE*, 5′-GGTCAGATCATGAAAATAGTTAAAGA-3' (forward) and
5′-ACTTATGTCGACTCAGAAATTAGG-3′ (reverse);
*ft*NadM, 5′-cggaggACATGTATGATATTTCAGTTT-3′ (forward) and
5′- cTATCACCCTGCAGTTATAGTTTTTTACC -3′ (reverse);
baNadD, 5′-GCACTCATGAGAAAAATTGGCATCATTG -3′ (forward) and
5′-GAAGTCTGCAGTCACGATTCATACAACC-3′ (reverse); and
*ba*NadE, 5′-GGACACATCATGACATTACAAGAACAGAT-3′ (forward) and
5′-TTTATGGTCGACTTATTTCCACCAATC-3′ (reverse).
The gel-purified PCR products were inserted into a pET-derived vector (1) containing the T7 promoter, His_6-tag, and TEV-protease cleavage site and were sequenced to confirm PCR accuracy.

Production and purification of *ft*NadE*, *ft*NadM, *ba*NadD, and *ba*NadE. All recombinant proteins were expressed as N-terminal fusions with a His_6-tag and a TEV-protease cleavage site in E. coli strain BL21/DE3. Cells were grown to an optical density at 600 nm of 0.8–1.0 at 37°C of LB medium. IPTG was added to 0.8 mM, and harvesting was performed after 12 h of shaking at 20°C. Proteins were purified from 6-liter cultures by chromatography on a Ni-NTA agarose column followed by gel filtration on a HiLoad Superdex 200 16/60 column (Pharmacia) with an AKTA FPLC system. The full protocol was similar to a procedure previously described (2). Proteins were purified to homogeneity as assessed by SDS-PAGE. Purified recombinant NadE enzymes from *Corynebacterium glutamicum* and *Helicobacter pylori* were obtained using the same techniques (unpublished results).

*Structural analysis of ftNadE**

For crystallization of *ft*NadE*, the 6xHis-tag was removed by treatment with TEV protease and the tag-removed protein was further purified with an ion exchange column Resource Q (GE Healthcare Life Sciences). The cocrystals of *ft*NadE* complexed with AMP, pyrophosphate (PPi), and Mg^{2+} were grown in a sitting-drop vapor diffusion setting at 20°C with 8 mg/ml protein mixed with an equal volume of reservoir solution containing 0.2M K/Na tartrate and 16% PEG 3350 in the presence of 5 mM ATP, 10 mM $MgCl_2$, and 20 mM NaMN. For data collection, *ft*NadE* crystals were transferred stepwise to a cryoprotection

solution containing the original reservoir solution and PEG 3350 increased to a final concentration of 40%. The diffraction data were collected on an R-AXIS IV image plate detector with X-ray generated by Rigaku FR-E SuperBright generator equipped with Osmic's VariMac focusing device and were processed with HKL2000 (3). The structure was solved by the molecular-replacement method of Molrep (4) using the *Bacillus subtilis* (*bs*NadE) structure (5) as the initial search model (pdb code 1kqp). The refinement and manual model building were performed with the program Refmac (6) of the CCP4 program suite(7) and COOT (8). The crystal data and current refinement statistics of *ft*NadE* structures are listed in SI Table 4.

Enzyme assays and steady-state kinetic analyses.

These assays were used to assess apparent values of kinetic parameters toward pyridine nucleotide substrates (NaMN, NMN, and NaAD at 10 μM–8 mM)) at constant saturating concentration of other substrates (2 mM ATP for all enzymes and 4 mM NH_4Cl for NadE enzymes). The amount of enzyme in the reaction mixture was maintained at a level between 0.1 and 500 μg/ml, leading to 1–10% substrate consumption within the incubation time. For HPLC assays, the linearity of response was assessed by the analysis of aliquots taken at 2–3 time points over the course of reaction. Apparent values of K_m and k_{cat} were calculated by fitting initial rates to a standard Michaelis–Menten model using the software Prism 4 (GraphPad), unless otherwise stated.

Continuous coupled assays - NaMN and NMN adenylyltransferase activity

The respective activities of NadD and NadM enzymes were measured with continuous assay coupling NAD formation to the alcohol dehydrogenase-catalyzed conversion of NAD to NADH as described (9) with slight modifications. Reactions were performed in a reduced volume of 100 uL using UV-transparent micro-cuvettes (BrandTech Scientific, Essex, CT) at 37 °C and monitored by the change in UV absorbance at 340 nm using a Beckman DU-800 spectrophotometer. Assay mixtures contained 2 mM ATP, 10 mM $MgCl_2$, 20 mM semicarbazide, 6 U/ml alcohol dehydrogenase, and 60 mM ethanol in 50 mM Hepes (pH 7.5). The reaction was started by adding either NMN or NaMN to 1 mM. To evaluate the NaMN-specific activity, an excess of pure recombinant NAD synthetase from *C. glutamicum* and NH_4Cl to 5 mM were also added. An NADH extinction coefficient of 6.22 mM^{-1} cm^{-1} was used for initial rate calculations using Multimode Detection software (Beckman).

Continuous coupled assay - NAD synthetase activity

The measurement of NAD synthetase (NADS) activity was determined as reported previously(10). Briefly, the reactions containing 2 mM ATP, 10 mM $MgCl_2$, 20 mM semicarbazide, 6 U/ml alcohol dehydrogenase, 60 mM ethanol, 5 mM NH_4Cl in 50 mM Hepes (pH 7.5) were initiated by adding NaAD to 1 mM.

Discontinuous (2-step) coupled assay - NMN synthetase activity

We developed a two-step spectrophotometric assay coupling the NMN synthetase activity to NADH formation via conversion of NMN to NAD by added excess of the purified recombinant *ft*NadM, followed by alcohol dehydrogenase-catalyzed conversion of NAD to NADH. The first step reaction (in 200 uL: 100 mM Hepes pH 7.5, 10 mM $MgCl_2$, 1 mM NaMN, 2 mM ATP, 5mM NH_4Cl) was started by the addition of NadE enzyme. After incubation at 37°C, the reaction was stopped by rapid cooling and removing of the active enzyme by microultrafiltration with Microcon YM-10 centrifugal filters (Amicon, Bedford, Mass.). A complete conversion of NMN into NADH was then accomplished by addition of one volume of the coupling buffer: 50 mM Hepes (pH 7.4), 20 mM Semicarbazide, 120 mM EtOH, 1.4 U of alcohol dehydrogenase and pure recombinant *ft*NadM. The mixture was

incubated at 25 °C for 20 min and NADH concentration was determined by absorbance at 340 nm (molar extinction of NADH used for all calculations was 6,220 M^{-1} cm^{-1}).

HPLC-based assay – NMN and NAD synthetase activities, and in vitro pathway reconstitution

A direct HPLC-based assay was used to directly assess and compare NMN synthetase and NAD synthetase activities of all NadE enzymes (including those from *C. glutamicum* and *H. pylori*), to determine steady-state kinetic parameters (for NaMN and NaAD) of *ft*NadE* and *ba*NadE enzymes and to monitor pathway reconstitution using mixtures of purified recombinant enzymes. Kinetic assays were carried out in 0.1 ml reaction mixtures in 96-well plates containing 50 mM Hepes (pH 7.5) with 10 mM $MgCl_2$ and 4 mM NH_4Cl. The enzymes *ft*NadE* and *ba*NadE were incubated with 2 mM ATP and varying concentrations (from 50 microM to 12.5 mM NaMN or NaAD at 37°C. For *in vitro* pathway reconstitution, mixtures of purified *ft*NadE* and *ft*NadM or *ba*NadD and *ba*NadE (3-100 μg ml^{-1} each) were incubated with 2 mM ATP, 1 mM NaMN, 10 mM $MgCl_2$ and 4 U/ml inorganic pyrophosphatase in 50 mM Hepes, pH 7.5 at 37 °C for 0.5-1 h and analyzed by ion-pair HPLC on LC-18T column (Supelco). Reactions were stopped by adding half-volume of ice-cold 1.2M perchloric acid ($HClO_4$). After 10 min at 4 °C, samples were centrifuged and brought to pH 6 by 0.8M K_2CO_3 addition. Proteins were removed from the supernatant by microultrafiltration and the filtrates were analyzed by RP-HPLC using a Shimadzu Prominence HPLC system with LC-10AD solvent delivery system, CBM-20AD system controller, SPD-20AD UV/Vis detector, SIL-20A auto sampler, CTO-20A column oven and DGU-20A3 on-line degasser. The separation was performed at room temperature on a Supelco LC-18-T (15 cm × 4.6 mm, 3 μm particle size) column equipped with Supelguard LC-18-T (2.0 cm × 4.0 mm, 5 μm particle size) guard column (Supelco, Bellefonte, PA), monitoring absorbance at 254 nm. Data were collected and processed by EZstart software package (Version 7.3). Chromatographic conditions and a standard separation are illustrated in Supplementary Fig.4. Molar areas were determined using calibration with standard solutions under the same chromatographic conditions.

NMN synthetase activity in cleared cellular lysates. Crude extracts of *F. tularensis* strain U112 wild-type and NadE* knockout mutant were prepared from mid log-phase grown cells as described above for protein purification. Briefly, cells were harvested, and resuspended for 20 min in a buffer with 1 mg/ml lisozyme, 2 mM PMSF, and 2 mM β-merchaptoethanol. After a cycle of thawing and sonication, cell debris was removed by centrifugation and the supernatant was probed for NMN synthetase activity (HPLC-based assay).

Mathematical Modelling of the Mixed Enzymatic Solution System

Mathematical model

A mathematical model describing a well-mixed enzymatic solution system, depicted in Scheme 1**,** is a set of standard kinetic mass balances [1]

$$\frac{d[A]}{dt} = V_0 - V_1 - V_3, \tag{1}$$

$$\frac{d[B]}{dt} = V_1 - V_2, \tag{2}$$

$$\frac{d[C]}{dt} = V_3 - V_4, \tag{3}$$

$$\frac{d[D]}{dt} = V_2 + V_4 - k_D \cdot [D]. \tag{4}$$

Here t is time, [A] is the concentration of NaMN, [B] is the concentration of NMN, [C] is the concentration of NaAD, and [D] is the concentration of NAD (the nomenclature of metabolite and enzyme names is provided in the main text and in Figure 1). V_0 is the constant influx of NaMN into the system and k_D is the degradation/utilization kinetics rate constant for NAD. The reaction rates V_1, V_2, V_3, and V_4, and the corresponding kinetic constants are provided in SI Table 5 and SI Table 6, respectively. The mathematical expressions for the kinetic rates (i.e. V_1, V_2, V_3, and V_4) are obtained using a standard Michaelis-Menten approach (11, 12).

Below the following two different modelling situations are considered in detail, (1) simulation of transient time courses in a *closed* well-mixed "test-tube" enzymatic solution system (i.e. when $V_0 = k_D = 0$) and (2) the analysis of the steady-state fluxes and the metabolite concentrations in an *open* "cellular subsystem" with a non-zero mass flow across the subsystem's systematic boundary. In this case, the nonzero values of V_0 and k_D are set so that [D] = 1 (mM) at the steady-state.

To relate the data in Table 1 and 2 here (i.e. k_i, K_i, i = 1, 2, 3, 4) to the corresponding kinetic parameters in Table 1 of the main text, we note that (k_1, K_1) = (k_{cat}, K_m) for *ft*NadE* (NaMN) and *ba*NadE (NaMN), respectively; (k_2, K_2) = (k_{cat}, K_m) for *ft*NadM (NaMN) and *ba*NadD (NMN), respectively; (k_3, K_3) = (k_{cat}, K_m) for *ft*NadM (NMN) and *ba*NadD (NaMN), respectively; and (k_4, K_4) = (k_{cat}, K_m) for *ft*NadE* (NaAD) and *ba*NadE (NaAD).

Transient time courses in the closed "test-tube" enzymatic system

In this case, the zero values of the parameters V_0 and k_D are used, $V_0 = k_D = 0$. At time t = 0, initial conditions [A_0] = 1 (mM) and [B_0] = [C_0] = [D_0] = 0 (mM) were always used. By summing up the equations (1) through (4) with zero V_0 and k_D, it can be shown that the total sum of metabolite concentrations is preserved and does not change in time t,

$$[A] + [B] + [C] + [D] = [A_0]. \tag{5}$$

Conservation relationship (5) is called a total *moiety* conserved pool. Mathematically, (5) means that differential equations (1) – (4) are linearly dependent and, therefore, to calculate the corresponding time courses in (1) – (4), only three differential equations, combined with the algebraic equation (5), are required. Specifically, equations (2) – (4) were integrated to calculate transient concentration profiles [B], [C], and [D], while concentration profile [A] of metabolite A was obtained from (5) using equations (6) – (9),

$$[A] = [A_0] - [B] - [C] - [D], \tag{6}$$

$$\frac{d[B]}{dt} = V_1 - V_2, \tag{7}$$

$$\frac{d[C]}{dt} = V_3 - V_4, \tag{8}$$

$$\frac{d[D]}{dt} = V_2 + V_4. \quad (9)$$

The dependence of V_1, …, V_4 on [A] is excluded from (7) – (9) using (6) substituted into the corresponding mathematical expressions for rates V_1 , …, V_4 given in Table 1.

To estimate the contribution of the two different routes, **Route II** utilizing enzymes *ft*NadE and *ft*NadM and **Route I** utilizing enzymes *ba*NadD and *ba*NadE, into the formation of the final product D (i.e. NAD), equation (9) was additionally replaced by two equations

$$\frac{d[D_1]}{dt} = V_2, \quad (10)$$

$$\frac{d[D_2]}{dt} = V_4. \quad (11)$$

Here $[D] = [D_1] + [D_2]$, D_1 can be interpreted as a "fraction" of metabolite D formed through flux V_2 (i.e. $A \xrightarrow{E_1} B \xrightarrow{E_2} D$) and D_2 is a "fraction" of D formed through V_4 (i.e. $A \xrightarrow{E_2} C \xrightarrow{E_1} D$). Equations (6) – (8), (10) and (11) were integrated using the Matlab© procedure *ode15s* with relative and absolute tolerances RelTal = AbsTol = 10^{-7}, respectively. All integration calculations were automatically terminated when the concentration $[D]$ of metabolite D reached ~90-99% of the initial concentration $[A_0]$ of metabolite A using a simple *event* procedure available through the Matlab© interface. The corresponding time courses are depicted in SI Figures 10 and 11. To relate SI Figure 10 and 11 to Fig. 3 (*a*, *b*) in the main text, we note that Figure 2(*a*) here corresponds to Fig. 11(*a*) in the main text, while Figure 11(c) here corresponds to Fig. 3(b) of the main text, respectively. We also note that vanishing concentrations of the intermediates do not assume that the corresponding fluxes leading to and from a vanishing intermediate are also vanishing. Specifically, although the concentration of intermediate B depicted in SI Figure 10(c) and (e) is negligible small compared to the other concentrations, the flux through B (i.e. fraction D1) is not small meaning that intermediate B is not accumulated in the mixture and it is instead converted to final product D rapidly.

From SI Figure 10, we find that in the case of organism *F* 100% of NAD is produced utilizing Route II when the concentration of E_1 is greater than the concentration of E_2, that is $[E_1]:[E_2] = 10:1$ (see SI Figure 10 (*a*) and (*b*)). In the other two cases, depicted in SI Figure 10 (*c*) – (*f*), both enzymatic routes are involved in the formation of NAD. However, such scenarios may be unlikely to happen in or could be highly inefficient for organism *F* as in this case it can take 15-150 times longer to produce NAD. Note that for organism *B*, Route I always prevails over Route II in the formation of NAD as seen from SI Figure 11.

The analysis of steady states in the open enzymatic system

To evaluate steady-state fluxes in the open enzymatic system, the non-zero values of parameters V_0 and k_D were set. Specifically, we used $V_0 = 10^{-3}$ (mM·s^{-1}) and $k_D = 10^{-3}$ (s^{-1}). After summing up equations (1) through (4) with non-zero values of V_0 and k_D, we obtain

$$\frac{d[D]}{dt} = V_0 - k_D \cdot [D]. \quad (12)$$

It follows from (12), that the steady state concentration $[D]$ of metabolite D is uniquely defined by the values of V_0 and k_D and $[D]$ is independent of the other kinetic parameters,

$$[D] = \frac{V_0}{k_D}. \quad (13)$$

Due to the choice of the specific values for V_0 and k_D, we have $[D] = 1$ (mM).

The steady-state values of metabolite concentrations and fluxes for organisms *F* and *B* with different ratios of enzyme concentrations E_1 and E_2 were obtained using a Matlab© numerical solver *fsolve* utilizing the Gauss-Newton method applied to the system of algebraic equations

$$V_0 - V_1 - V_3 = 0, \quad (14)$$

$$V_1 - V_2 = 0, \quad (15)$$

$$V_3 - V_4 = 0, \quad (16)$$

$$V_2 + V_4 - k_D \cdot [D] = 0. \quad (17)$$

The equations (14) – (17) are obtained from the differential equations (1) – (4) by equating the time derivatives to zero values, $d[A]/dt = d[B]/dt = d[C]/dt = \mathrm{d}[D]/dt = 0$ ($\mathrm{mM \cdot s^{-1}}$). Appropriate approximations for the solutions to (14) – (17), used as initial conditions for the Newton-like solver fsolve, were generated by the direct integration of equations (1) – (4) over a long time interval, $t_{\mathrm{end}} = 10^4$ (s). The stability of the corresponding steady-state solutions was calculated using Matlab© function *eig* utilized to calculate the eigenvalues of the Jacoby matrix of partial derivations of the linearization of (14) – (17) at the solution. The Jacoby matrix was directly available from *fsolve* function. The corresponding steady state concentrations and fluxes are summarized in Table 3 for different values of enzyme concentrations ratios in organisms *F* and *B*. An example of eigenvalues (i.e. λ_k, $k = 1, \ldots, 4$) calculated to evaluate the stability is given below for organism *F* with $[E_1]:[E_2] = 10:1$. The negative real parts of the eigenvalues are indicative of the asymptotical stability of the algebraic solutions to (14) – (17) viewed as the corresponding steady states in the full system (1) – (4),

$$\lambda_1 = -1.00 \cdot 10^{-3},$$
$$\lambda_2 = -2.51 \cdot 10^{-3},$$
$$\lambda_3 = -3.05 \cdot 10^{-4},$$
$$\lambda_4 = -8.58 \cdot 10^{-5}.$$

From the comparison of the steady-state fluxes, we find that for organism *F*, Route II, $A \xrightarrow{E_1} B \xrightarrow{E_2} D$, is exclusively utilized in the formation of NAD when $[E_1]:[E_2] = 10:1$ and both routes 1 and 2 are active when $[E_1]:[E_2] = 1:1$. We could not calculate any reasonable distributions of steady-state metabolite concentrations and fluxes in the case of $[E_1]:[E_2] = 1:10$ which may be indicative of the biological infeasibility of this case for organism *F*. The modelling data for organism *B*, provided in Table 3, show that in all the three cases, NAD is solely produced utilizing Route I only.

Francisella tularensis nadE knockout mutant and complementation study*

To address the in vivo function of *ft*NadE* we used a nadE transposon mutant of *F. tularensis* subsp. *novicida* strain U112. The transposon T20 in the mutant tnfn1_pw060328p05q173 is inserted in the *nadE* gene (FTN_1278) between nucleotide (nt) 414 and nt 415. The insertion was confirmed by PCR and sequencing using the transposon-specific primer KAN-125 and the flanking primer NADE-ECO. The same approach was used to analyze the viable *nadM* transposon mutant. The transposon T20 in the mutant tnfn1_pw060328p06q193 is inserted in the *nadM* gene (FTN_0483) between nt 565 and nt 566. The insertion was confirmed by PCR and sequencing using the transposon-specific primer KAN-125 and the flanking primer NADM-SAL. The mutants tnfn1_pw060328p05q173 and tnfn1_pw060328p06q193 were obtained from a comprehensive sequenced-defined transposon mutant library(13). The PCR reactions were performed with these primers:
KAN-125, 5'-AACGCAGACCGTTCCGTGGC-3',
NADE-*Eco*, 5'-ATGAATTCTGGGCAAAGAATTGCTGAAATAACTAAGG-3', and
NADM-*Sal*, 5'-ATGTCGACGGGTCATTAAAGCTTGTATTTAGGGAGC-3'. For complementation study the *nadE* gene was PCR-amplified from *F. tularensis* subsp. *novicida* genomic DNA with primers
NADE-*NcoI* (CGCGCGCCATGGGCATGAAAATAGTTAAAGATTTTAGTCCTAAAGA) and NADE-*EcoRI* (CGGAATTCTCAGAAATTAGGAGTTAAAGCTAATTTTCTCT). The

PCR fragment was digested with *NcoI* and *EcoRI*, and ligated into pKEK894 (14) digested similarly. The new resulting plasmid was named pKEK1210 (p*nadE*). Cloning was performed into *E.coli* strain DH5α. *F. tularensis* subsp. *novicida* strains were grown on TSM (tryptic soybean media), TSAP (tryptic soybean agar plates) supplemented with 0.1% cysteine, 25 mg/ml ferrous sulfate, 25 mg/ml sodium pyruvate, and 25 mg/ml sodium metasulfite, or on Chamberlain's defined medium (CDM)(15). Antibiotics were used at following concentrations: kanamycin 50 μg/ml, and tetracycline 10 μg/ml. Plasmid pKEK1210 was transformed into Δ*nadE* mutant (tnfn1_pw060328p05q173) (13) via electroporation(16). Transformed bacteria were then plated on media selective for tetracycline. A selected clone in which the plasmid pKEK1210 was confirmed (PCR, plasmid digestion and sequencing) was denoted KKF302 (Δ*nadE* + p*nadE*).

In vivo assessment of NAD biosynthetic intermediates.

F. tularensis strain U112 and *B. anthracis* strain Ames were grown in rich media (Trypticase Soy Broth and Luria Bertani, respectively) to log phase (OD_{600nm} ~1) and harvested by centrifugation. To assess relative abundance of the NMN intermediate in the *F. tularensis* wild type and NadE* knockout mutant, cells were grown in defined medium (Chamberlain) with 200 uM nicotinamide. Perchloric acid (PCA) extraction of pyridine nucleotides was adapted from Maharjan *et al.* (17). The cells were washed twice with cold PBS, followed by two cycles of freezing and thawing. Cells were then resuspended in 1:50 volume of MilliQ water, centrifuged, and extracted with 1:500 volume of 50% (V/V) ice-cold perchloric acid. After brief vortexing, the mixture was kept on ice for 15 min. Cell debris was removed by centrifugation, and supernatant was neutralized with 5N KOH; the resulting supernatants were removed and the extracts adjusted to pH 6.5. Extracts were aliquoted and stored at –20°C. NMN and NaAD intermediates were identified by HPLC analysis as described for the HPLC-based assay. In order to provide an accurate quantisation of these metabolites, these samples were subjected to enzymatic depletion of NMN and NaAD content by using an excess amount of *ft*NadM and *ba*NadE that would convert both intermediates to NAD in the proper buffer conditions. Total enzymatic depletion of intermediates was tested and optimized by adding exogenous NMN and NaAD at 100 uM in the presence or absence of the enzymes. Net NMN and NaAD concentrations were determined by subtracting samples' peaks from the corresponding peaks of the enzymatically depleted samples (see SI Fig. 11 for an example of NMN quantisation). For the enzymatic depletion of NMN and NaAD, 80 uL of extracts were diluted in 200 uL of buffer containing 50 mM Hepes (pH 7.5), 10 mM $MgCl_2$, 4 mM NH_4Cl, 2 mM ATP, and supplemented with an excess amount of *ft*NadM and *ba*NadE recombinant enzymes.

2 Tables and Figures

SI Table 1. Functional reconstruction of NAD biosynthesis and salvage pathways in a set of selected bacterial genomes.

Genome	Variant	De novo pathway: from Asp to NaMN			Salvage I: from nicotinamide or nicotinate to NaMN		From NaMN to NAD				Salvage II: from nicotinamide or nicotinamide ribose to NMN			
							Route I		Route II					
		ASPOX	QSYN	QAPRT	NAM	NAPRT	NaMNAT	NADS	NMNS	NMNAT	RNK	PnuC	NMPRT	
		nadB	*nadA*	*nadC*	*pncA*	*pncB*	*nadD*	*nadE*	*nadE*	*nadM*	*nadR*	*nadR*	*pnuC*	*nadV*
Conventional NaMN-NaAD-NAD pathway with de novo biosynthesis (a)														
Escherichia coli K12	**1.1.1.1**	2545	736	109	1851	916	640	1723			4298	4298	737	
Erwinia carotovora	**1.1.1.1**	668	3569	2442	1996	1526	3358	844			4163	4163	3636	
Pseudomonas aeruginosa	**1.1.1.1**	762	1005	4524	4915	4916,	4914	4917				1957	1958	
Pseudomonas putida	**1.1.1.1**	1414	1221	778	2212	4803	4745	4804				2833	2834	
Pseudomonas fluorescens	**1.1.1.1**	4142	7219	2968		3208	7530	3207				7505	2549	
Bacillus anthracis	**1.1.1.0**	**4305**	**4303**	**4304**	**155**	**557**	**4208**	**1831**					**190**	
Vibrio cholerae	**1.1.1.0**	980	2724	872	1633	639	1344	1343					671	
Bacillus clausii	**1.1.1.0**	1509	1511	1510	429	3941	1602	2455						
Bacillus halodurans	**1.1.1.0**	1218	1220	1219	3777	3249	1326	2285						
Bacillus subtilis	**1.1.1.0**	2790	2788	2789	3179	3178	2567	314						
Carboxydothermus. hydrogenoformans	**1.1.1.0**	2555	2556	2554	539		604	1486						
Clostridium difficile	**1.1.1.0**	2477	2476	2478	3518	3067	2098	1853						
Desulfitobacterium sp.	**1.1.1.0**	293	2486	294	1173	916	3137	917						
Exiguobacterium sp.	**1.1.1.0**	271	269	270	1390	1389	2783	2691						
Geobacillus kaustophilus	**1.1.1.0**	2735	2733	2734	669	668	2614	2693						
Listeria monocytogenes	**1.1.1.0**	2014	2016	2015	2561	1084	1480	1085						
marine actinobacterium	**1.1.1.0**	2539	2540	2538	1403	1721	2605	1679						
Neisseria gonorrhoeae	**1.1.1.0**	1646	1645	1643	1749	472	1328	554						
Nocardia farcinica	**1.1.1.0**	1846	1845	1847	1119	1120	1404	4155						
Corynebacterium efficiens	**1.1.1.0**	?	1116	1115	2385	2412	2257	2428						
Corynebacterium glutamicum	**1.1.1.0**	?	366	365	1664	1668	2167	1682						
Fusobacterium nucleatum	**1.1.1.0**	602	601	603		932	1708	1778						
Bacillus B-14905	**1.1.1.0**	1935	1933	1934		853	1337	852						
Leifsonia xyli	**1.1.1.0**	?	1096	1054		810	193	748						
Shewanella oneidensis	**1.0.1.1**	1244	2121	395			1087	1842						1809
Alteromonas macleodii	**1.0.1.0**	2200	843	3806			1341	2177						
Helicobacter hepaticus	**1.0.1.0**	17	1839	1833			351	1008						
Thiomicrospira denitrificans	**1.0.1.0**	1610	2028	2029			1383	1142						
Pseudoalteromonas haloplanktis	**1.0.1.0**	790	1975	370			881	144						
Wolinella succinogenes	**1.0.1.0**	1467	1180	1179			625	191						
Shewanella sp. PV-4	**1.0.1.0**	3517	3630	2462			3656	327						
Colwellia psychrerythraea	**1.0.1.0**	4266	1627	4670			1581	3712						
Candidatus Pelagibacter ubique	**1.0.1.0**	?	1302	1301			1185	93						
Helicobacter mustelae	**1.0.1.0**	?	1532	1533			1585	1209						
Helicobacter pylori	**1.0.1.0**	?	1344	1343			1325	325						
Vibrio fischeri	**1.0.1.0**	2094	814	2184			3340	3341					3210	
Conventional NaMN-NaAD-NAD pathway without de novo biosynthesis (b)														
Oenococcus oeni	**0.1.1.1**				703	47	65	240			53	53	1055	813
Lactococcus lactis	**0.1.1.1**				966	1132	1131	1134			2041	2041	2343	
Leuconostoc mesenteroides	**0.1.1.1**					120	793	121			98	98	99	
Streptococcus pneumoniae	**0.1.1.0**			2093	1437	1276	1590	1275					1672	
Streptococcus pyogenes	**0.1.1.0**			150	1368	1275	226	1274					1022	
Lactobacillus plantarum	**0.1.1.0**				2161	473	1268	474					468	
Campylobacter coli	**0.1.1.0**				1049	2028	1423	127						
Campylobacter jejuni	**0.1.1.0**				198	533	1624	851						
Campylobacter lari	**0.1.1.0**				468	45	682	331						
Campylobacter upsaliensis	**0.1.1.0**				977	1412	936	218						
Enterococcus faecalis	**0.1.1.0**				2980	2450	2676	2449						
Genome	**Variant**	ASPOX	QSYN	QAPRT	NAM	NAPRT	NaMNAT	NADS	NMNS	NMNAT	RNK	PnuC	NMPRT	
		nadB	*nadA*	*nadC*	*pncA*	*pncB*	*nadD*	*nadE*	*nadE*	*nadM*	*nadR*	*nadR*	*pnuC*	*nadV*
Mesoplasma florum	**0.1.1.0**				386	591	421	193						
Mycoplasma mycoides	**0.1.1.0**				996	653	417	415						
Lactobacillus acidophilus	**0.1.1.0**				1338	148	1525	149						
Oceanobacillus iheyensis	**0.1.1.0**				568	391	1985	392						
Pediococcus pentosaceus	**0.1.1.0**				1080	1171	1530	1172						
Staphylococcus aureus	**0.1.1.0**				2675	1782	1469	1781						
Tropheryma whipplei str. Twist	**0.1.1.0**				692	623	469	405						
Tropheryma whipplei TW08/27	**0.1.1.0**				677	611	277	343						
Buchnera aphidicola	**0.1.1.0**					347	426	173						
Mycoplasma hyopneumoniae	**0.1.1.0**					491	375	372						
Mycoplasma penetrans	**0.1.1.0**					939	520	195						
Mycoplasma pulmonis	**0.1.1.0**					483	335	623						
Ureaplasma parvum serovar	**0.1.1.0**					280	476	467						
Mycoplasma genitalium	**0.1.1.0**						246	398						37
Mycoplasma pneumoniae	**0.1.1.0**						336	563						47
Flavobacteria sp.	**0.1.1.0**			1034			2549	1800				2195	2196	
Unconventional NaMN-NMN-NAD pathway (c)														
Francisella tularensis Schu S4	**1.0.2.1**	**1160**	**1162**	1161					**1334**	**933**			**164**	**1282**
Mannheimia succiniciproducens	**0.1.2.1**					**1776**			**1775**		**164**	**164**	**185**	
Actinobacillus succinogenes	**0.1.2.1**					ZP_00732388			ZP_00732389		ZP_00732632	ZP_00732632	ZP_00733245	

SI Table 1 caption

This condensed subsystem spreadsheet (modified from "NAD and NADP cofactor biosynthesis global" subsystem at http://anno-3.nmpdr.org/anno/FIG/subsys.cgi) shows gene patterns of NAD biosynthesis and salvage routes in a subset of representative bacterial genomes corresponding to those used for phylogenetic analysis of NadE family ("short" form without a glutamine amidotransferase domain (10) (18) (19). Rows indicate species with completely sequenced genomes integrated in The SEED database (except *Actinobacillus succinogenes* 130Z, draft assembly at http://www.jgi.doe.gov), while genes and assigned functional roles within a metabolic pathway are shown as columns. Proteins are represented by abbreviated SEED identification numbers, except those for *Actinobacillus succinogenes* where IDs are provided as in NCBI (http://www.ncbi.nlm.nih.gov/); "?" - inferred by pathway analysis but a gene is unknown (cannot be projected by homology). Genes clustered on the chromosome (operons) are outlined by matching background colours. Genes (fusion proteins) encoding more than one functional role in the subsystem are underlined. The second column reflects a classification of organisms (genomes) using a four-number variant code. Each position of the variant code reflects the presence (usually 1 and in some cases "2" to capture alternatives) or absence (0) of a subsystem module (pathway) as it appears in the top row. Functional roles are abbreviated as follows: ASPOX, L-aspartate oxidase (EC 1.4.3.16); QSYN, Quinolinate synthetase (EC 4.1.99.-); QAPRT, Quinolinate phosphoribosyltransferase [decarboxylating] (EC 2.4.2.19), NAMNAT, Nicotinate-nucleotide adenylyltransferase (EC 2.7.7.18); NMNAT, Nicotinamide-nucleotide adenylyltransferase of NadM or NadR family (EC 2.7.7.1); NMNAT_M, Nicotinamide-nucleotide adenylyltransferase, NadM family (EC 2.7.7.1); ADPRP, ADP-ribose pyrophosphatase (EC 3.6.1.13); NADS, NAD synthetase (EC 6.3.1.5); NMNS, NMN synthetase (EC 6.3.1.-); NAM, Nicotinamidase (EC 3.5.1.19); NAPRT, Nicotinate phosphoribosyltransferase (EC 2.4.2.11); NMPRT, Nicotinamide phosphoribosyltransferase (EC 2.4.2.12); PNUC, Ribosyl nicotinamide transporter, pnuC-like; RNK, Ribosylnicotinamide kinase (EC 2.7.1.22).

SI Table 2 | Conservation of NAD biosynthetic machinery among the 7 sequenced variants of *F. tularensis* deposited in GenBank.

Francisella Tularensis strains	Genomes	De novo pathway, Asp→→→NaMN			(Novel) Route II, NaMN→NMN→NAD		Niacin Salvage, Nm→NAD	REF
		ASPOX (NadB)	QSYN (NadA)	QAPRT (NadC)	NMNS (NadE)	NMNAT/ADPRP (NadM)	NMPRT (NadV)	
FSC 198	AM286280	FTF1467c	FTF1469c	FTF1468c	FTF1259 (100)	FTF0386 (99)	FTF5134c	(20)
FTA	CP000803	FTA_1475	FTA_1477	FTA_1476	FTA_0724 (99)	FTA_0479 (100)	FTA_0613	
LVS	**AM233362**	**FTL_1388**	**FTL_1390**	**FTL_1389**	**FTL_0685 (100)**	**FTL_0452 (100)**	**FTL_0579**	
OSU18	CP000437	FTH_1350	FTH_1352	FTH_1351	FTH_0687 (100)	FTH_0449 (100)	FTH_0579	(21)
Schu 4	AJ749949	FTT1467c	FTT1469c	FTT1468c	FTT1259 (100)	FTT0386 (99)	FTT1534c	(22)
U112	CP000439	FTN_0694	FTN_0692	FTN_0693	FTN_1278 (99)	FTN_0483 (98)	FTN_1443	(23)
WY96-3418	CP000608	FTW_0631	FTW_0629	FTW_0630	FTW_0685 (99)	FTW_1688 (100)	FTW_0395	(24)

Genes implicated in NAD biosynthesis/salvage/recycling pathways of the eight sequenced strains of *Francisella* are shown by locus tags and genomes by GenBank Accession numbers. Enzyme abbreviations are described in the caption of SI Table 1. Numbers in brackets are the amino acid sequence identities (%) of NadE and NadM with respect to the enzymes of our reference strain, *F. tularensis* subsp *holarctica* LVS. Genes clustered in the chromosome are highlighted by the gray background. Schu S4, FSC198, and WY96-3418 belong to subsp *tularensis;* LVS, OSU18, and FTA to subsp *holarctica*, U112 to subsp *novicida*; This analysis suggests that all of these strains implement the same set of NAD pathways, including the novel NaMN→NMN→NAD pathway validated in this study for *F. tularensis* ssp *holarctica*.

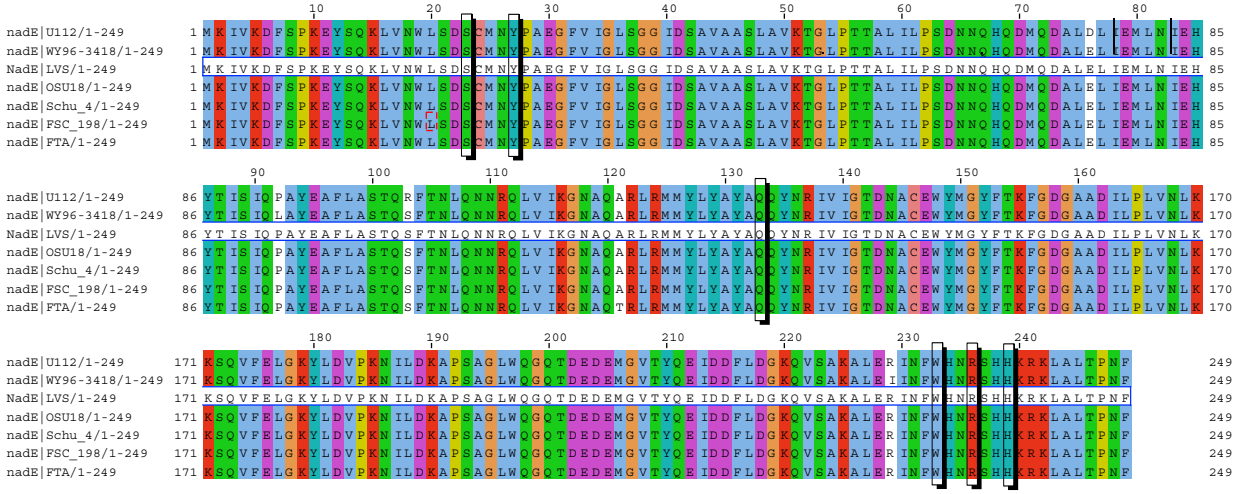

SI Fig. 1 | Conservation of NadE* enzymes among the 7 fully sequenced variants of *F. tularensis* deposited in GenBank. Multiple sequence alignment was performed using *Muscle* (25) and edited with *Jalview* (26). Positions with a percentage of identity above 90% are coloured-coded according to *Clustalx* (27)output standards. None of the few amino acid substitutions between the seven strains affect residues (marked by blocks, see text for description) that according to our 3D analysis could substantially contribute to catalysis or/and specificity.

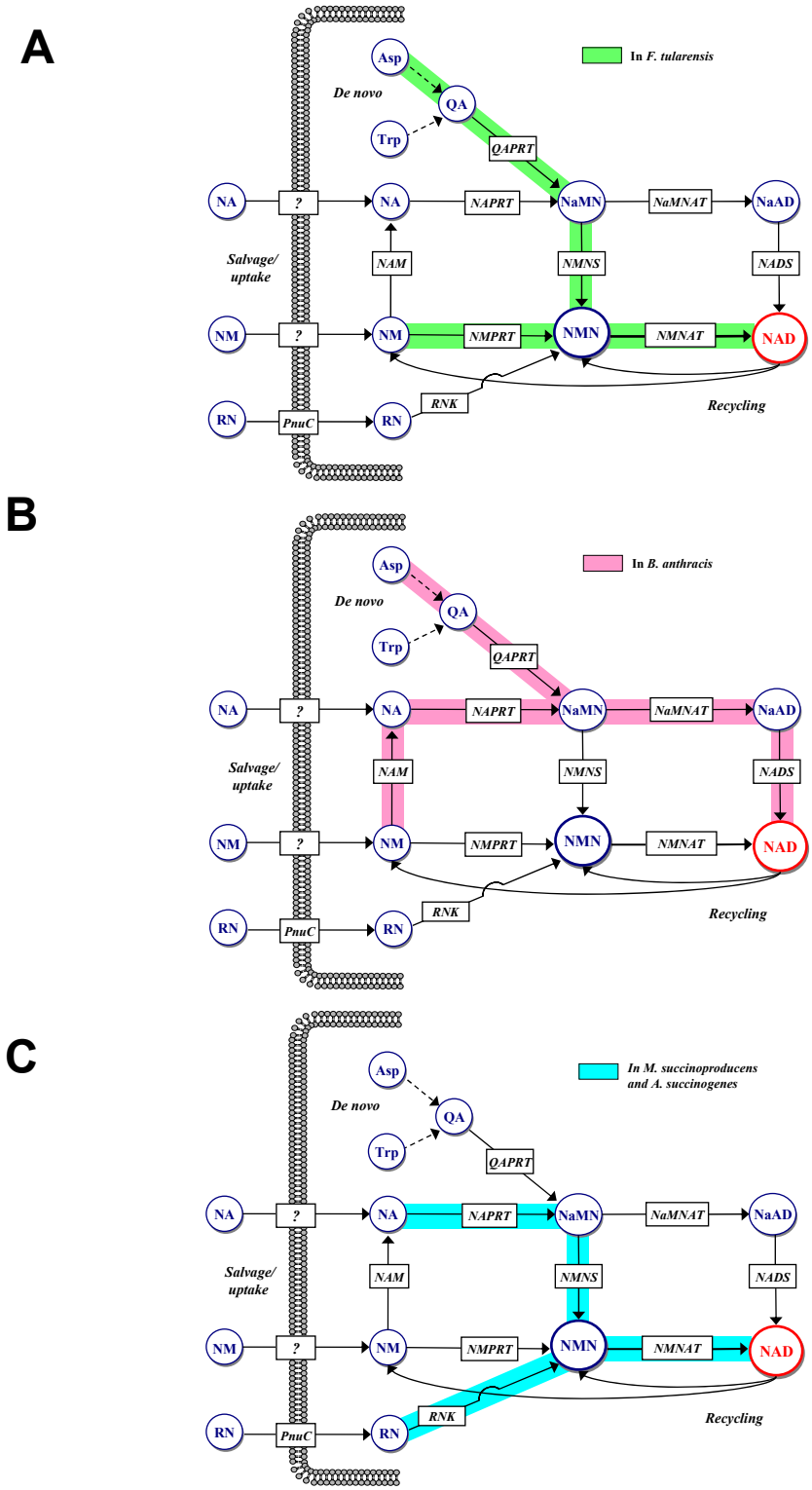

SI Fig. 2. NAD biosynthesis subsystem diagram. Functional roles are shown by abbreviations in boxes (as defined in Supplementary Table 1). Intermediates are shown by abbreviations in circles. Asp, *L*-aspartate; Trp, *L*-tryptophane, NA, nicotinic acid; NM, nicotinamide; NMR, *N*-ribosylnicotinamide; NaMN, nicotinate mononucleotide; NMN, nicotinamide mononucleotide; NaAD, deamido-NAD. Dashed arrows indicate multistep transformations. Thick coloured bars outline individual pathways present in *F. tularensis* (**A**), *B. anthracis* (**B**) and *M. succinoproducens/A. succinogenes* (**C**) as inferred by the presence or absence of respective genes (SI Table 1)

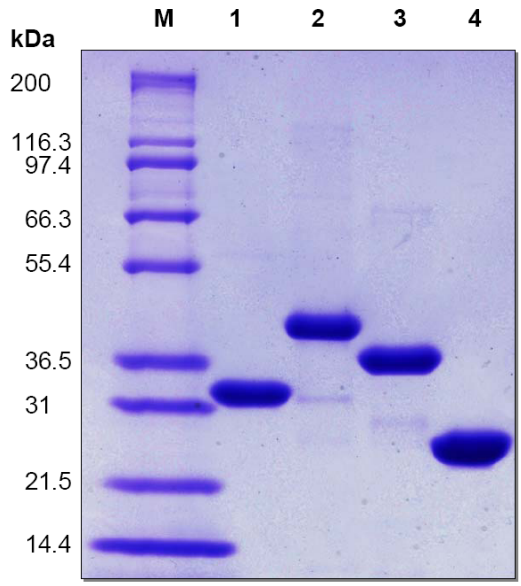

SI Fig. 3 | SDS-PAGE of *F. tularens*is and *B. anthracis* enzymes.
Analysis in 10 - 20% gradient SDS-PAGE of purified recombinant enzymes used for kinetics and pathway reconstitution studies : *Lane M*, molecular weight standards; *Lane 1*, *ft*NadE*; , Lane 2, *ft*NadM; Lane 3, *ba*NadE; Lane 4, *ba*NadD (5 µg each)

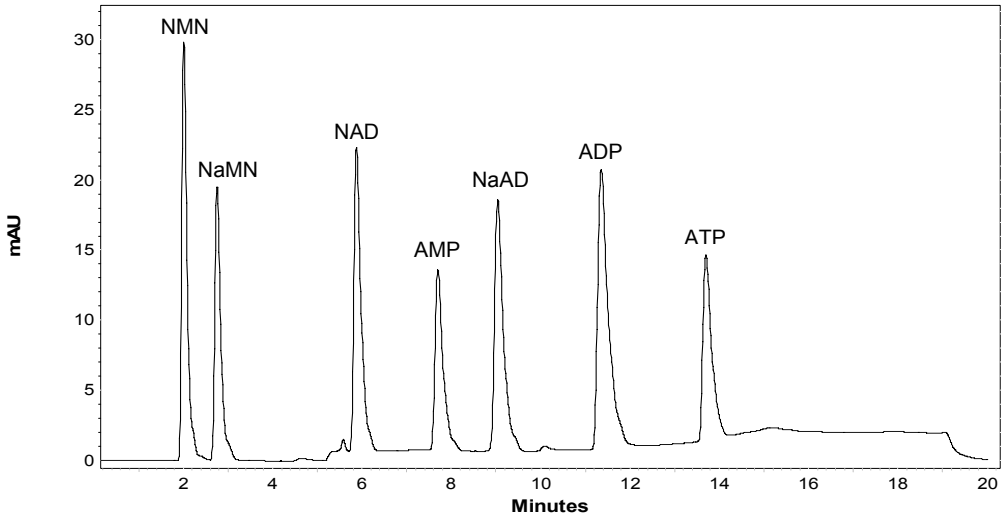

SI Fig. 4 | HPLC-based analysis used for kinetic studies of NadE enzymes and to monitor the entire pathway reconstitution. Standard separation of NaMN, NMN, NAD, NaAD, AMP, ADP and ATP (0.2-1 nmoles). The flow rate was 1 ml/min. Solvent A was a mixture of 0.1 M potassium phosphate, pH 6.0 and 8 mM tetrabutylammonium bromide and solvent B was 30% methanol in buffer A. B,. The solvent gradient consisted of 3 min at 95% A, 2 min at up to 30 % B, 5 min at up to 60% B, 3 min at up to 100 % B, hold for 4 minutes, and then returned to starting conditions for 3 min.

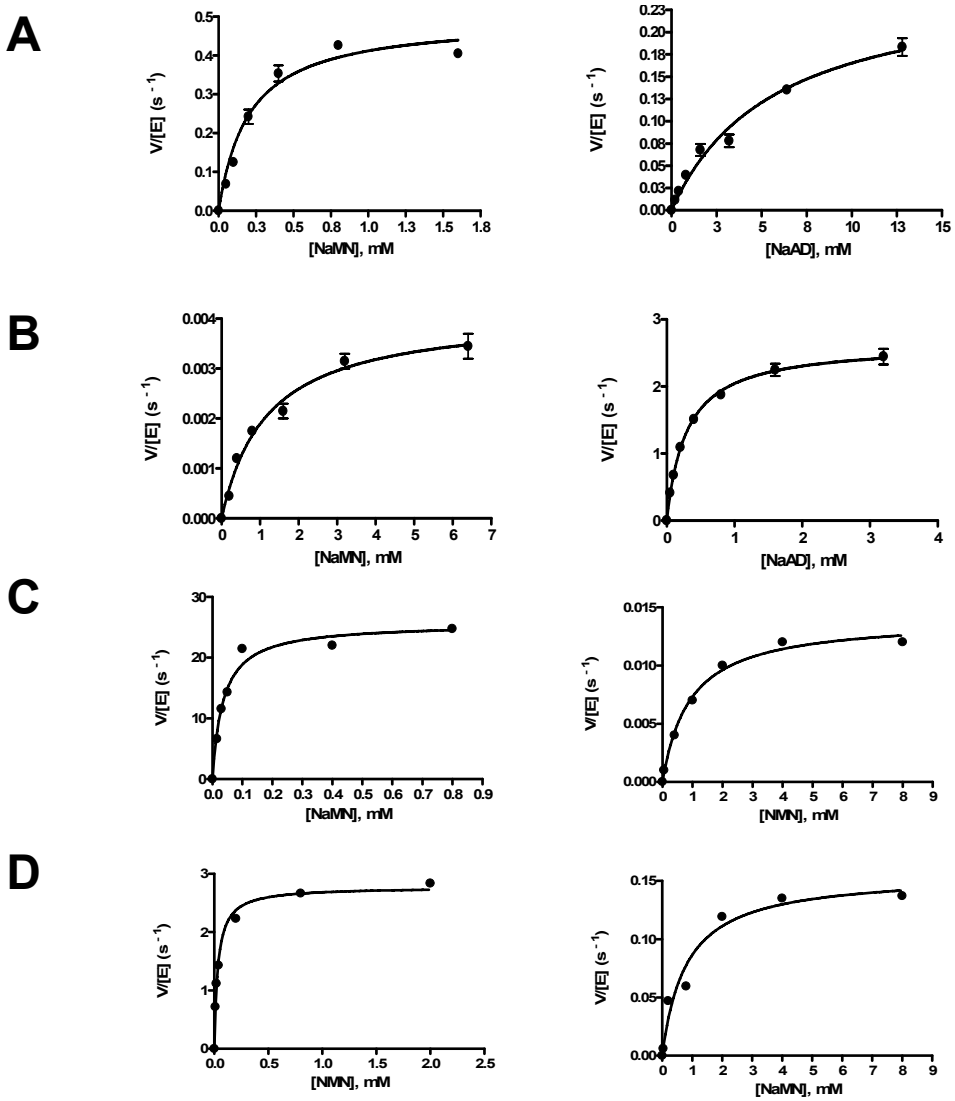

SI Fig. 5. Plots of initial rates versus substrate concentration obtained for *ft*NadE* (A), *ba*NadE (B), *ba*NadD (C), *ft*NadM (D). Apparent kinetic parameters for the respective pyridine nucleotide substrates were determined at saturating ATP (for NMN-NaMN adenylyltransferase activity assays) or at saturating ATP and NH_4Cl (for NaMN-NaAD synthetase assays). Data were fit to the Michaelis-Menten equation. Note that up to 20-30% substrate inhibition was observed for *ft*NadE* NMN synthetase activity at NaMN concentration above 3 mM. Therefore a limited data set (up to 1.2 mM) was used for the approximation by a simple Michaelis-Menten model. Fitting the entire data set (up to 6.4 mM) using a substrate inhibition model resulted in similar K_m and k_{cat} values (data not shown).

SI Table 3 | *C. glutamicum* and *H. pylori* NadE substrate preference.

Enzyme	NAD synthetase (U/mg)	NMN synthetase (U/mg)	Ratio
C. glutamicum NadE	3.27 ± 0.04	(0.76 ± 0.08) x 10^{-3}	4302
H. Pylori NadE	0.19 ± 0.01	(0.18 ± 0.03) x 10^{-3}	1055

The relative substrate preferences were assessed for NadE enzymes from *C. glutamicum* and *H. pylori* by measuring their specific amidation activities at fixed 2 mM concentrations of NaMN and NaAD by HPLC analysis.

SI Table 4. Crystal data and refinement statistics of *ft*NadE* complex

Data statistics	
Space group	$P2_12_12_1$
Cell dimensions	*a*=50.43Å, *b*=126.45Å, *c*=152.54Å
Resolution (Å)	50-1.85
Total observations	294774
Unique observations	79468
Completeness (%)	94.0 (70.3)[1]
R_{sym}[2] on *I*	0.044 (0.356)
Mean I/σ	19.8 (2.6)
Refinement	
R_{cryst}[3]	0.184
R_{free}[4]	0.233
Number of Protein atoms	7564
Ligands	4 AMP, 4 PPi, 8 Mg, 4 Na
Number of waters	812
Ave. B-factors (Å^{-1})	
Protein	25.5
Ligands	19.1
Water	33.5
Rmsd bond length (Å)	0.014
Rmsd bond angle (°)	1.394

[1] The values in the parenthesis are for the highest resolution shells 1.92-1.85Å.
[2] $R_{sym} = \Sigma_{hkl} \Sigma_i |I_i(hkl) - \langle I(hkl) \rangle| / \Sigma_{hkl} \Sigma_i I_i(hkl)$

[3] $R_{cryst} = \Sigma_{hkl} ||F_{obs}| - k|F_{calc}|| / \Sigma_{hkl} |F_{obs}|$, where F_{obs} and F_{calc} are the observed and calculated structure factors, respectively.

[4] R_{free} is calculated the same way as R_{cryst} using randomly selected 5% of the reflections that were omitted from the refinement.

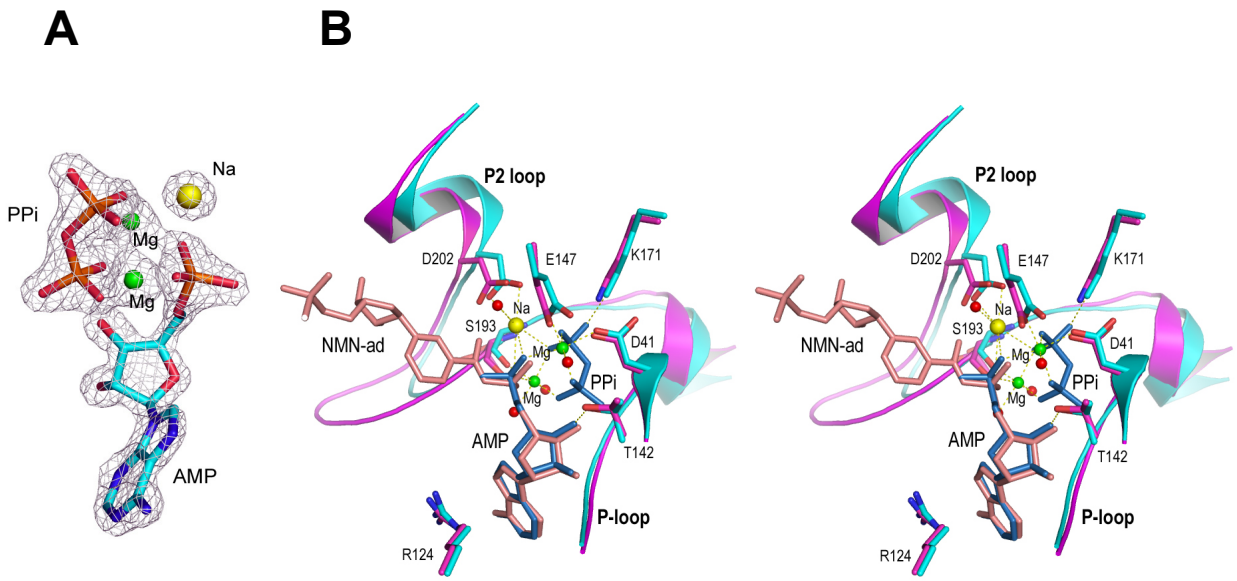

SI Fig. 6 Ligand binding in the 3D structure of NadE active site. A**,** The difference (Fo-Fc) electron density for the bound ligand and metal ions in *ft*NadE* complex structure. The map is contoured at 3σ level. B, Stereo view of superimposed catalytic site in *ft*NadE* (cyan) and *bs*NadE (magenta).

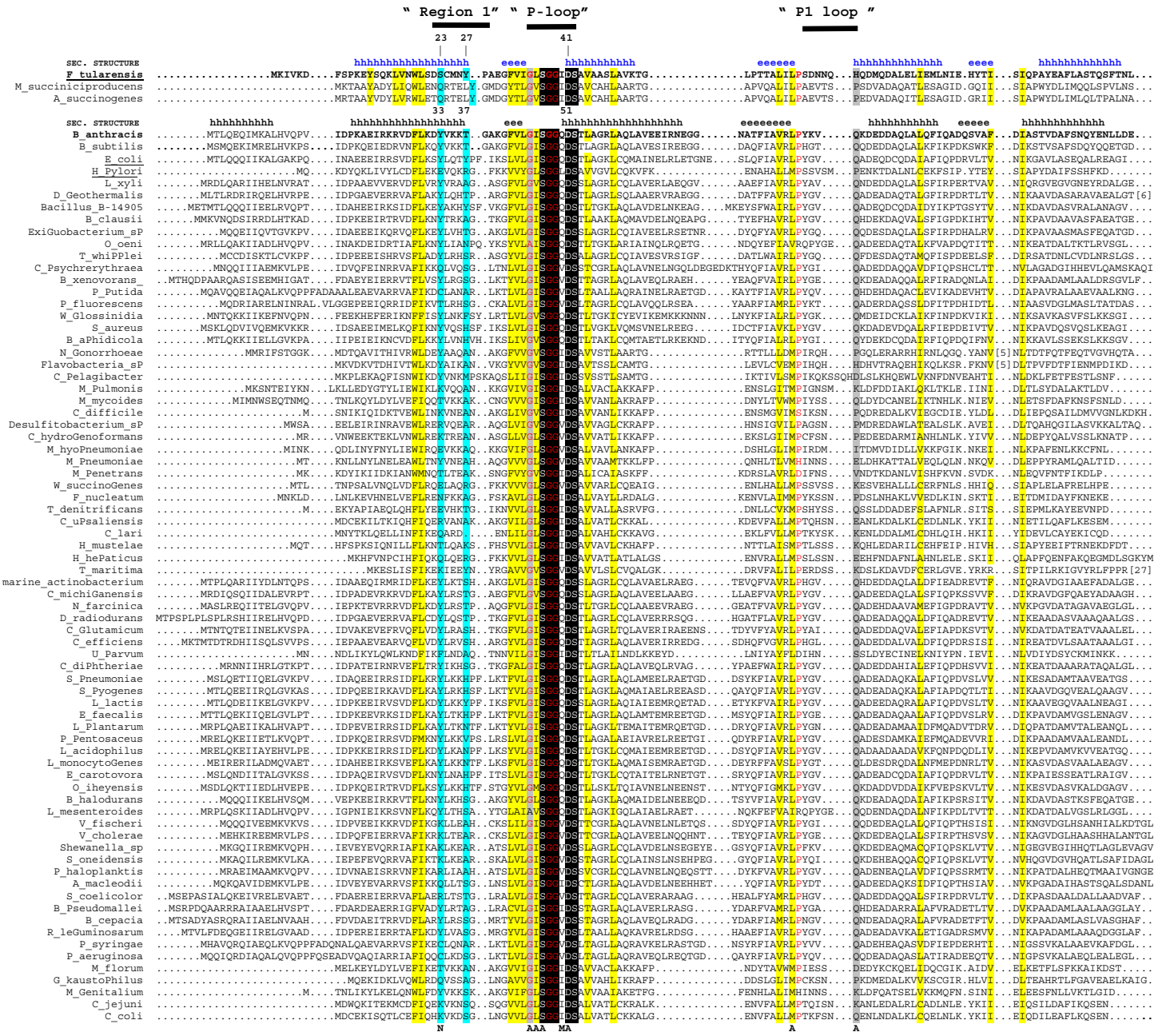
" Region 1"
" P-loop"
" P1 loop "
" P2 loop "
SEC. STRUCTURE
F_tularensis
M_succiniciproducens
A_succinogenes
B_anthracis
B_subtilis
E_coli
H_Pylori
L_xyli
D_Geothermalis
Bacillus_B-14905
B_clausii
ExiGuobacterium_sP
O_oeni
T_whiPPlei
C_Psychrerythraea
B_xenovorans_
P_Putida
P_fluorescens
W_Glossinidia
S_aureus
B_aPhidicola
N_Gonorrhoeae
Flavobacteria_sP
C_Pelagibacter
M_Pulmonis
M_mycoides
C_difficile
Desulfitobacterium_sP
C_hydroGenoformans
M_hyoPneumoniae
M_Pneumoniae
M_Penetrans
W_succinoGenes
F_nucleatum
T_denitrificans
C_uPaliensis
C_lari
H_mustelae
H_hePaticus
T_maritima
marine_actinobacterium
C_michiGanensis
N_farcinica
D_radiodurans
C_Glutamicum
C_efficiens
U_Parvum
C_diPhtheriae
S_Pneumoniae
S_Pyogenes
L_lactis
E_faecalis
L_Plantarum
P_Pentosaceus
L_acidophilus
L_monocytoGenes
E_carotovora
O_iheyensis
B_halodurans
L_mesenteroides
V_fischeri
V_cholerae
Shewanella_sp
S_oneidensis
P_haloplanktis
A_macleodii
S_coelicolor
B_Pseudomallei
B_cepacia
R_leGuminosarum
P_syringae
P_aeruginosa
M_florum
G_kaustoPhilus
M_Genitalium
C_jejuni
C_coli

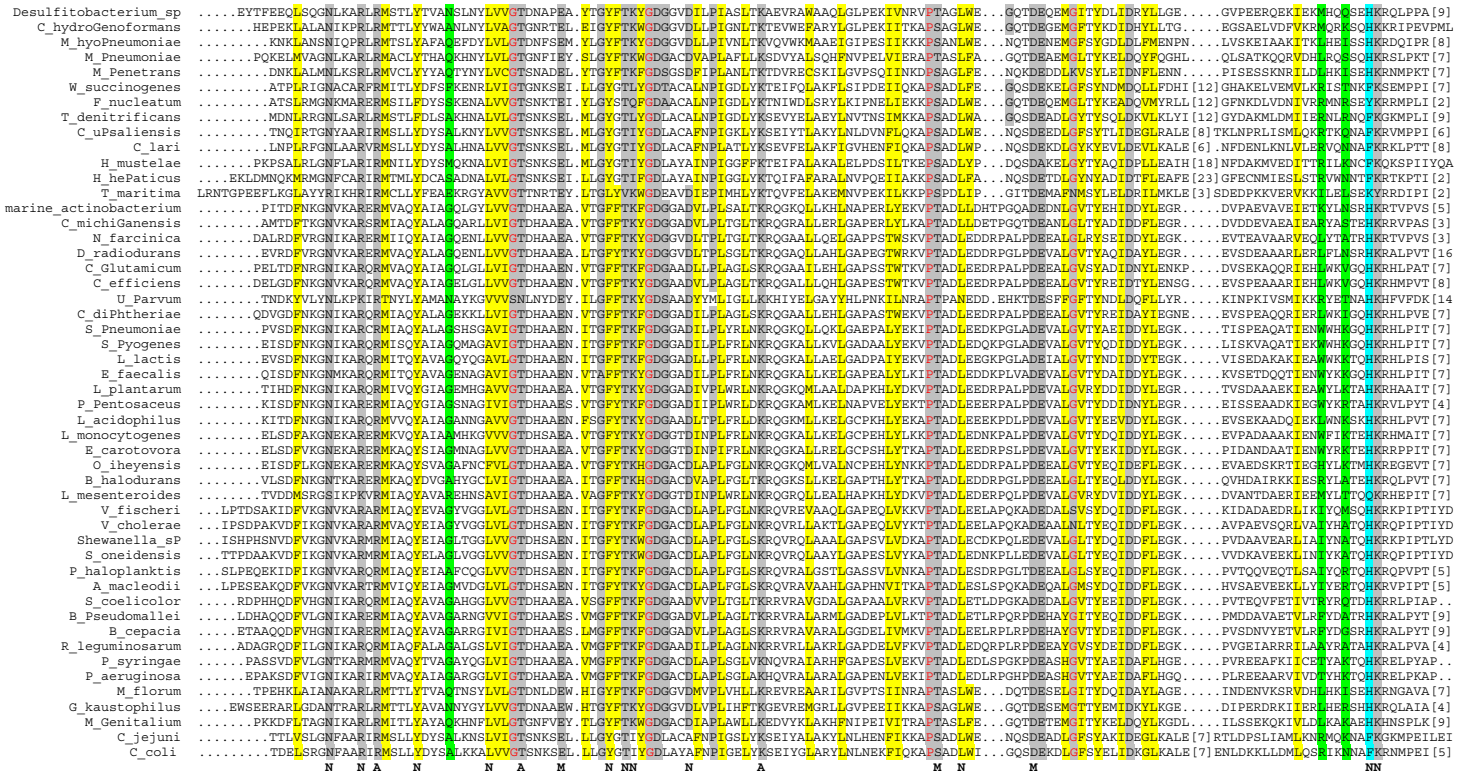

SI Fig. 7 | Multiple sequence alignment of representative bacterial NadE enzymes. Complete organism names for all NadE representatives are provided in SI Table 1. Those with known 3D structure are underlined. The signature "P-loop" motif residues are highlighted in black. Locations of secondary structure elements are marked for *ft*NadE* and *bs*NadE with "h" for helix and "e" for strand. Conserved small or polar residues are highlighted in gray. Uncharged residues in mainly hydrophobic sites are highlighted in yellow. Residues that interact with ATP, NAD, or metal ions are indicated by letter A, N or M, respectively, at the bottom of the alignment. Residues that are different between *ft*NadE* and *bs*NadE in their adenosyl binding site (shaded by cyan) and nicotinosyl binding site (shaded by green) are indicated.

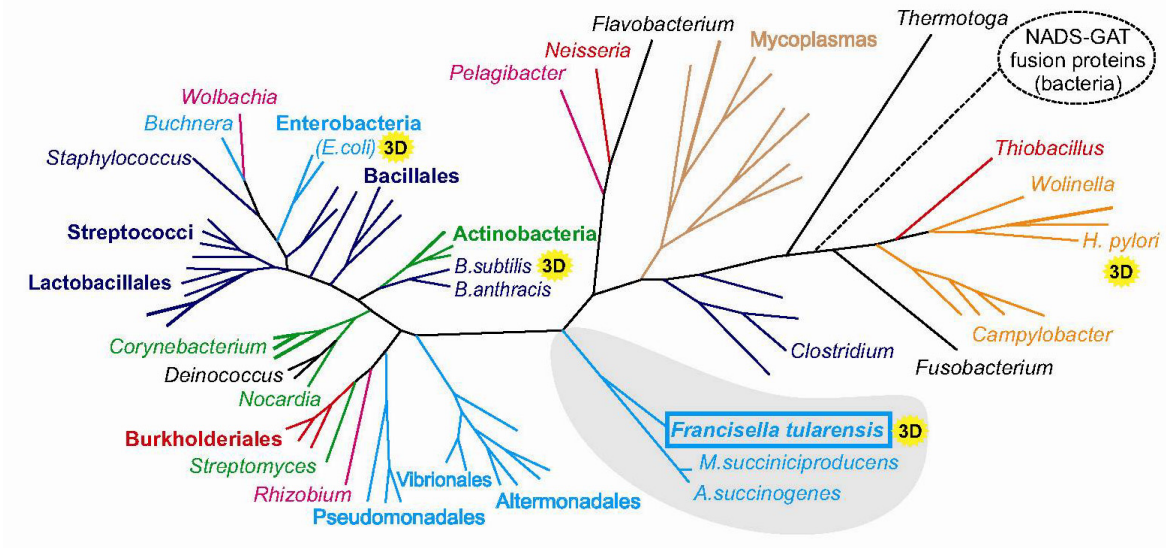

SI Fig. 8 | Maximum-likelihood phylogenetic tree of bacterial NAD synthetase family. Constructed based on 67 bacterial representatives of NadE family that do not contain a glutamine-amidotransferase domain (reduced from the original set of ~200 sequences by a single linkage clustering method with 75% identity threshold to decrease redundancy). Color coding denotes major taxonomic groups: α-proteobacteria (magenta), β-proteobacteria (red), γ-proteobacteria (cyan), ε-proteobacteria (orange), Bacillus/Clostridium group (dark blue), Mycoplasmatales (brown). Experimentally characterized NAD synthetases with solved tertiary structures are marked by "3D". A distinct NMN synthetase branch containing *F. tularensis* NadE and two orthologs from *M. succinoproducens* and *A. succinogenes* is outlined by grey background. An approximate branching point for a more divergent group of NAD synthetases containing an additional glutamine-amidotransferase domain (NADS-GAT) is shown by a dashed line.

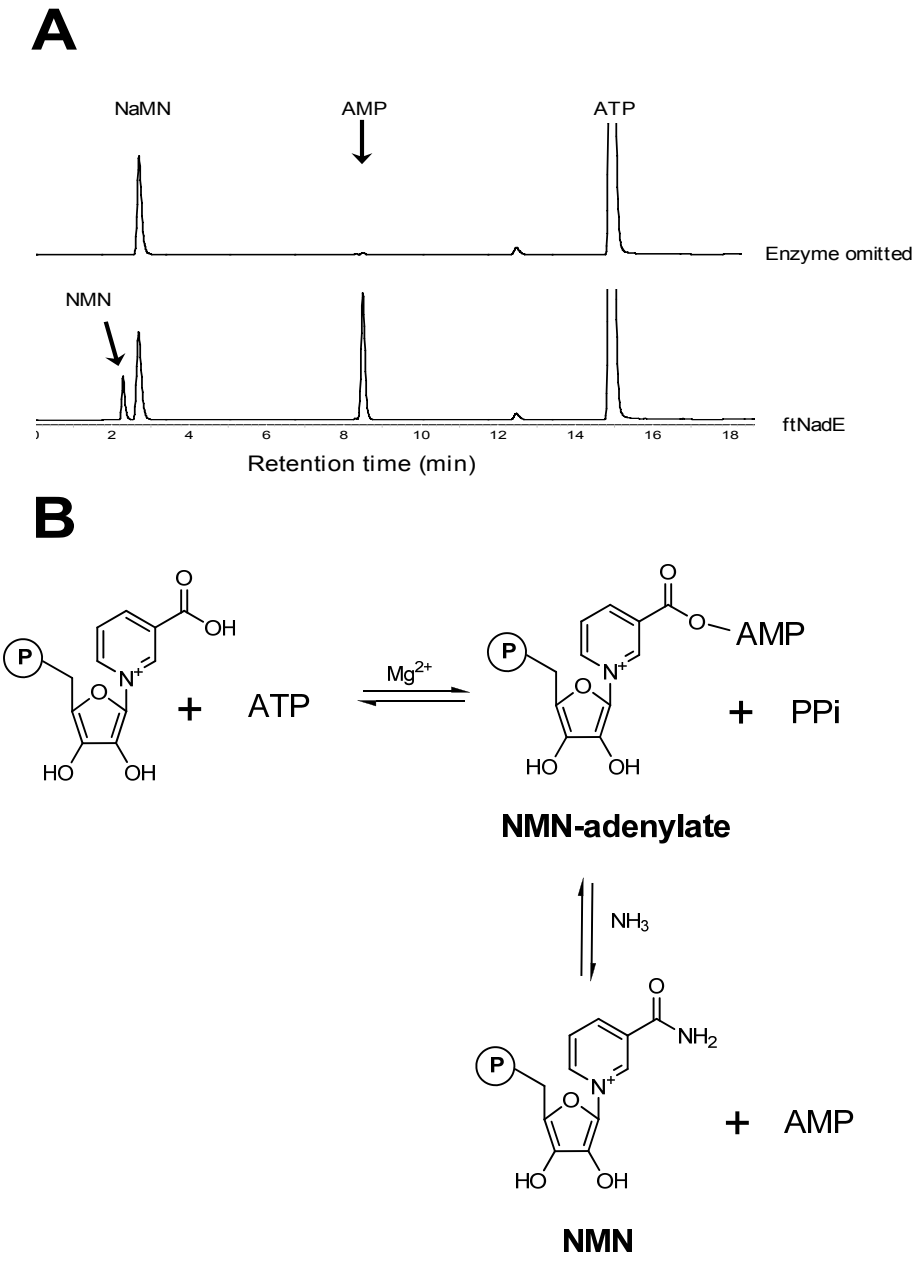

SI Fig.9 | Direct verification of *ft*NadE* catalyzed conversion of NaMN to NMN. (A) direct verification of novel NMN synthase activity of *F. tulariensis nadE* gene product. Shown are the HPLC (traces at 254 nm) of reaction mixtures containing 2 mM ATP, 1 mM NaMN, 4 mM NH_4Cl, 10 mM Mg^{2+} in the absence or presence of 4 uM *ft*NadE* after 1 h of incubation. Positions corresponding to NMN and AMP products are indicated by arrows. (B) The proposed mechanism of reaction catalyzed by NMN synthetase by analogy with the known mechanism of NAD synthetase

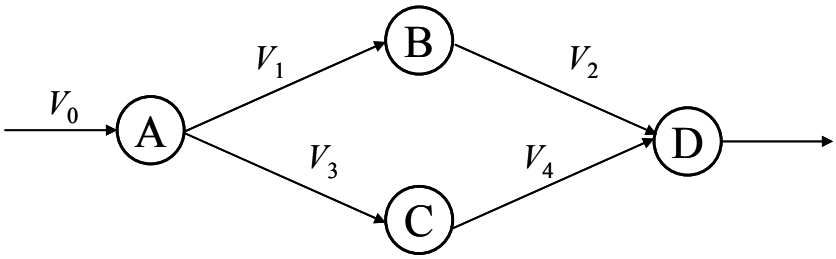

Scheme 1. An enzymatic system described by the model (1) – (4). The system is analyzed for two important organisms, *Francisella tularensis* (organism ***F***) and *Bacillus anthracis* (organism **B**), see the main text for more details. Here **A** is the universal *nicotinic acid mononucleotide precursor* (**NaMN**), **B** is *nicotinamide mononucleotide intermediate* (**NMN**), **C** – *nicotinic acid dinucleotide* (**NaAD**), **D** – *nicotinamide adenine dinucleotide* (**NAD**). Reaction **1** is catalyzed by *NMN synthetase* (***ft*NadE**), reaction **2** is catalyzed by *NMN adenylyl transferase* (***ft*NadM**), reaction **3** is catalyzed by *NaMN adenylyl transferase* (***ba*NadD**), and reaction **4** is catalyzed by *NAD synthetase* (***ba*NadE**). V_0 is an influx into the open system; the pathway is modelled as a closed system (e.g. a test-tube) when V_0 is absent (i.e. when $V_0 = 0$ and the utilization of D is absent). Route I, A→**C**→D, and Route II, A→**B**→D, corresponds to Route I and Route II depicted in Fig.1 of the main text, respectively.

SI Table 5. Kinetic rates for enzymatic reactions as in Scheme 1.

№	Enzyme Name	Reaction Rate
1	NMN synthetase	$V_1 = \frac{k_1 \cdot [E_1] \cdot [A]}{K_1 \cdot (1 + [C]/K_4) + [A]}$
2	NMN adenylyl-transferase	$V_2 = \frac{k_2 \cdot [E_2] \cdot [B]}{K_1 \cdot (1 + [C]/K_4) + [A]}$
3	NaMN adenylyl-transferase	$V_3 = \frac{k_3 \cdot [E_2] \cdot [A]}{K_1 \cdot (1 + [C]/K_4) + [A]}$
4	NAD synthetase	$V_4 = \frac{k_4 \cdot [E_1] \cdot [C]}{K_1 \cdot (1 + [C]/K_4) + [A]}$

SI Table 6. Enzymatic kinetic parameters for the reaction rates as in SI Table 5.

Parameters	Francisella tularensis	Bacillus anthracis
$k1$ (1/sec)	0.5	0.004
$K1$ (mM)	0.2	1.18
$k2$ (1/sec)	2.8	0.014
$K2$ (mM)	0.034	0.94
$k3$ (1/sec)	0.16	25.6
$K3$ (mM)	0.81	0.04
$k4$ (1/sec)	0.25	2.64
$K4$ (mM)	5.8	0.29

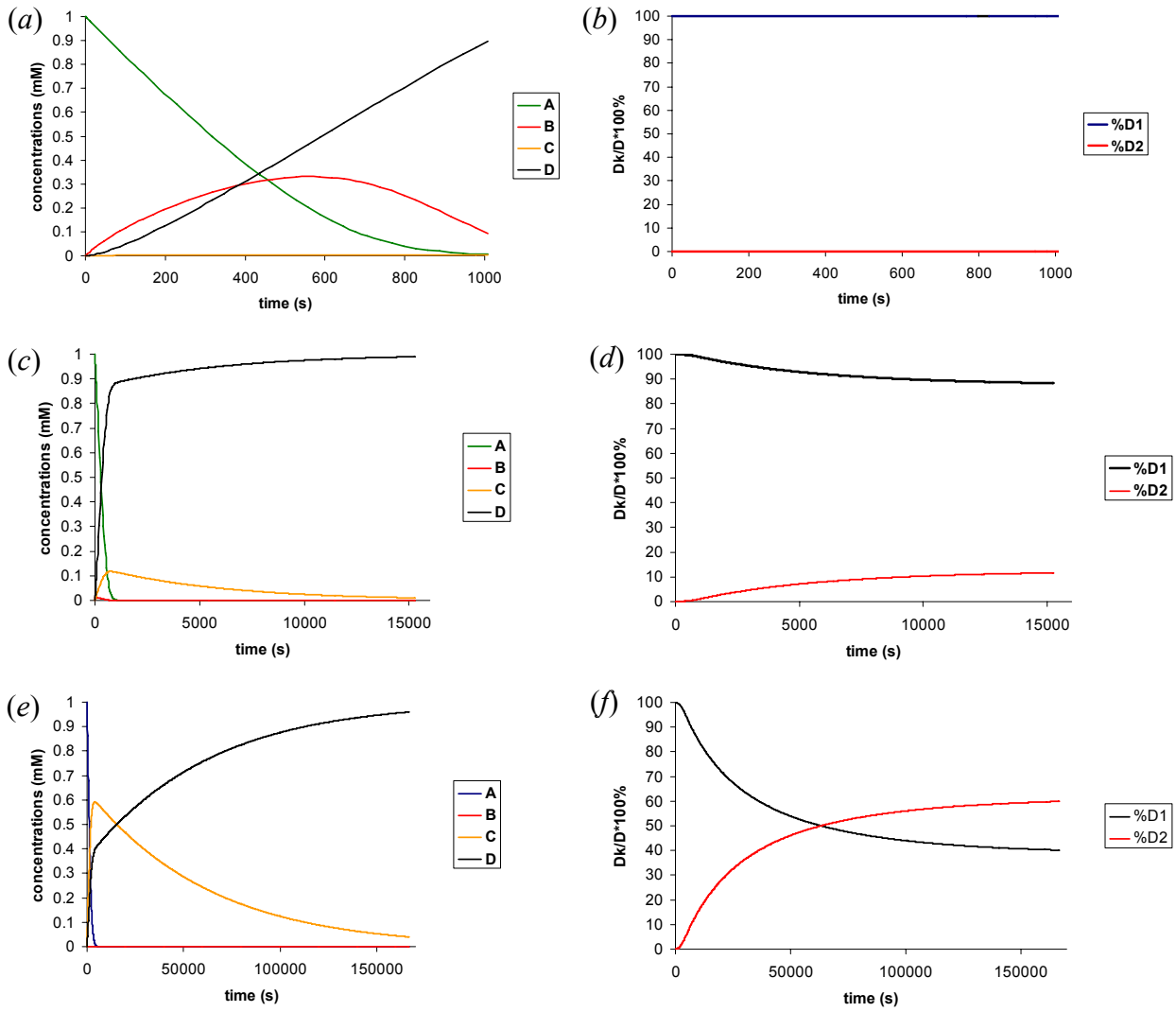

SI Figure 10. Transient processes for the metabolite concentrations for organism *F*. (*a*), (*b*) $[E_1] : [E_2] = 10 : 1$, $[E_1] = 4 \cdot 10^{-3}$ (mM); (*c*), (*d*) $[E_1] : [E_2] = 1 : 1$, $[E_1] = 4 \cdot 10^{-3}$ (mM) (*e*), (*f*) $[E_1] : [E_2] = 1 : 10$, $[E_1] = 4 \cdot 10^{-4}$ (mM). $\%D_k(t) = [D_k](t)/[\mathrm{D}](t)$.

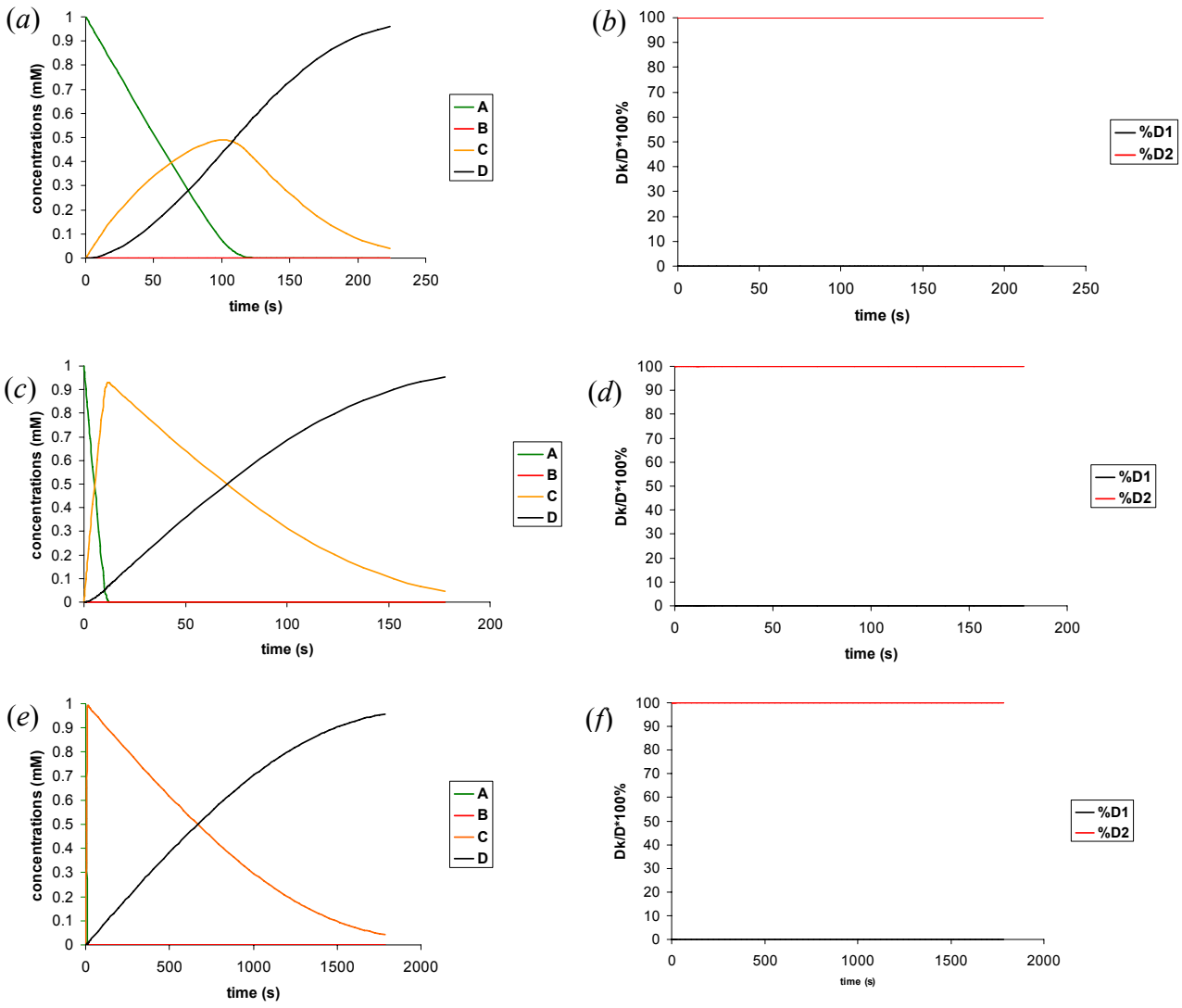

SI Fig. 11. Transient processes for the metabolite concentrations for organism *B*. (*a*), (*b*) $[E_1] : [E_2] = 10 : 1$, $[E_1] = 4 \cdot 10^{-3}$ (mM); (*c*), (*d*) $[E_1] : [E_2] = 1 : 1$, $[E_1] = 4 \cdot 10^{-3}$ (mM) (*e*), (*f*) $[E_1] : [E_2] = 1 : 10$, $[E_1] = 4 \cdot 10^{-4}$ (mM). $\%D_k(t) = [D_k](t)/[\mathrm{D}](t)$ ($k = 1$ and 2).

SI Table 7. Steady state concentrations and fluxes in organisms *F* and *B*.

Organism F	Organism B
1. E1=0.004 (mM) and E2 = 0.0004 (mM)	
concentrations fluxes	**concentrations fluxes**
$[A] = 0.20$ (mM) $V_1 = 9.99\cdot10^{-4}$ (mM·s^{-1})	$[A] = 4.38\cdot10^{-3}$ (mM) $V_1 = 5.35\cdot10^{-8}$ (mM·s^{-1})
$[B] = 0.35$ (mM) $V_2 = 9.99\cdot10^{-4}$ (mM·s^{-1})	$[B] = 1.02\cdot10^{-2}$ (mM) $V_2 = 5.44\cdot10^{-8}$ (mM·s^{-1})
$[C] = 0.016$ (mM) $V_3 = 1.37\cdot10^{-6}$ (mM·s^{-1})	$[C] = 3.04\cdot10^{-2}$ (mM) $V_3 = 1.00\cdot10^{-3}$ (mM·s^{-1})
$[D] = 1.00$ (mM) $V_4 = 1.37\cdot10^{-6}$ (mM·s^{-1})	$[D] = 1.00$ (mM) $V_4 = 1.00\cdot10^{-3}$ (mM·s^{-1})
2. E1=0.004 (mM) and E2 = 0.004 (mM)	
$[A] = 0.20$ (mM) $V_1 = 8.83\cdot10^{-4}$ (mM·s^{-1})	$[A] = 3.95\cdot10^{-4}$ (mM) $V_1 = 4.84\cdot10^{-9}$ (mM·s^{-1})
$[B] = 0.36$ (mM) $V_2 = 8.83\cdot10^{-4}$ (mM·s^{-1})	$[B] = 8.50\cdot10^{-5}$ (mM) $V_2 = 5.02\cdot10^{-9}$ (mM·s^{-1})
$[C] = 1.53$ (mM) $V_3 = 1.17\cdot10^{-4}$ (mM·s^{-1})	$[C] = 3.03\cdot10^{-2}$ (mM) $V_3 = 1.00\cdot10^{-3}$ ((mM·s^{-1}))
$[D] = 1.00$ (mM) $V_4 = 1.17\cdot10^{-4}$ (mM·s^{-1})	$[D] = 1.00$ (mM) $V_4 = 1.00\cdot10^{-3}$ (mM·s^{-1})
3. E1=0.0004 (mM) and E2 = 0.004 (mM)	
The concentrations of metabolite C becomes very large, $[C] > 100$ (mM) while $[D] = 1$ (mM).	$[A] = 3.94\cdot10^{-4}$ (mM) $V_1 = 2.84\cdot10^{-11}$ (mM·s^{-1})
	$[B] = 4.81\cdot10^{-7}$ (mM) $V_2 = 2.84\cdot10^{-11}$ (mM·s^{-1})
	$[C] = 5.18$ (mM) $V_3 = 1.00\cdot10^{-3}$ (mM·s^{-1})
	$[D] = 1.00$ (mM) $V_4 = 1.00\cdot10^{-3}$ (mM·s^{-1})

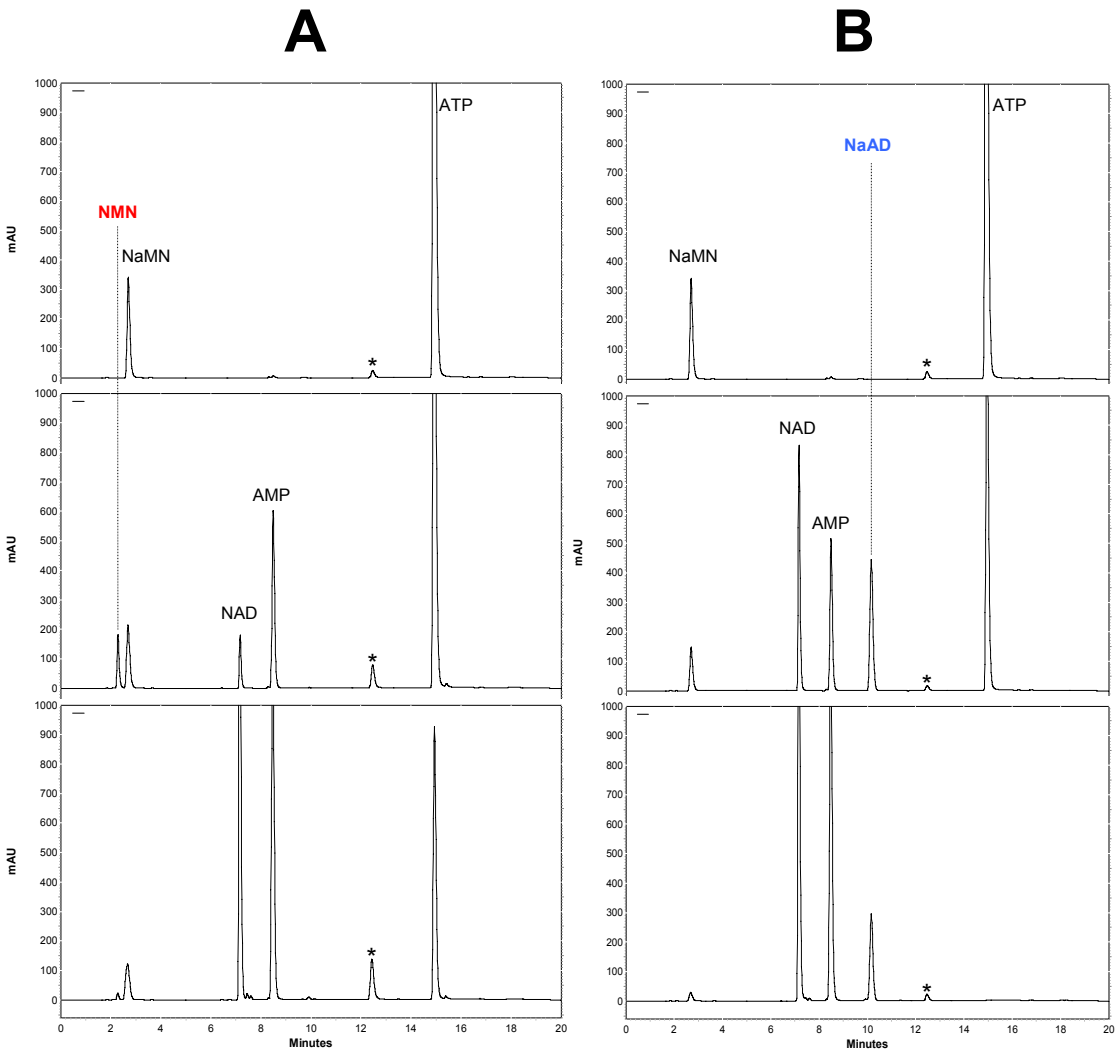

SI Fig. 12.Complete HPLC traces of NAD pathway reconstitution experiments. Individual chromatograms of pathway reconstitution experiments presented in Fig. 3c,3d and performed as described in Methods. Upper, middle and lower traces show progression of *in vitro* NAD biosynthesis at time 0, 30 and 60 minutes in *Francisella tularansis* [(A), NaMN→NMN→NAD] and *Bacillus anthracis* systems [(B), NaMN→NaAD→NAD]. Peaks corresponding to pathway intermediates, NMN and NaAD, are indicated by dotted vertical lines. An extra peak corresponding to ADP (spontaneous hydrolysis of ATP) is marked by asterisk.

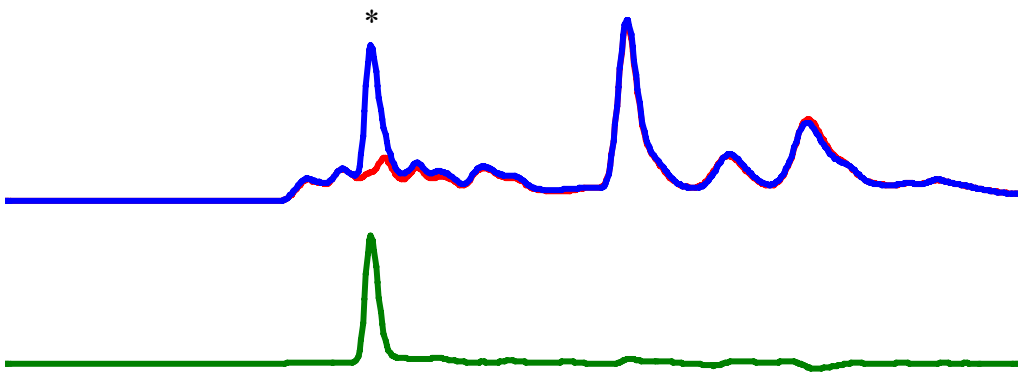

SI Fig. 13. In vivo assessment of NAD intermediates. Shown are partial HPLC profiles of NAD biosynthetic intermediates in extracts of *F. tularensis* strain U112 prior (blue) and after (red) enzymatic depletion of NMN (*) by NMN adenylyltrasferase. A subtracted profile (green) enables an accurate quantitation of cellular NMN amount. A similar strategy, with an excess of NAD synthetase as a metabolite-depleting enzyme was followed to quantitate NaAD (not shown).

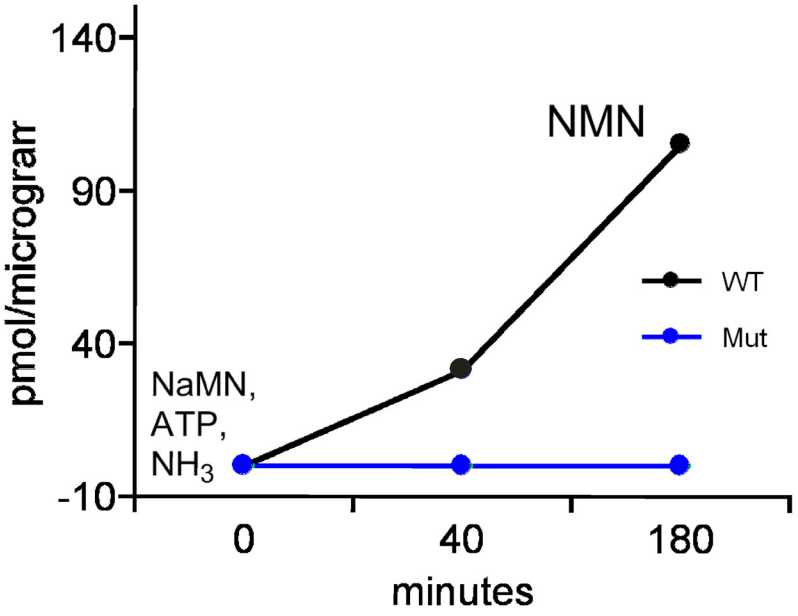

SI Fig.14. Measurement of NMN synthetase activity in crude extracts of *F. tularensis* strain U112: comparison between WT and NadE* knockout mutant. Incubation of 70 ug total protein extract with 1 mM NaMN, 2 mM ATP and 4 mM NH_4Cl yelds accumulation of NMN intermediate over time, while no formation of NMN is detected for the *ft*NadE* knockout mutant. This result confirms the in vivo NMN synthetase function of *ft*NadE*.

Supplementary discussion

Phylogenetic distribution and a possible evolutionary scenario of the newly identified NMN synthetase

The phylogenetic distribution of the newly identified NMN synthetase, a signature enzyme of the Route II (NaMN→NMN→NAD) pathway, appears to be rather limited. A comparative sequence analysis of all representatives of the NadE family from the 650 completely sequenced genomes integrated in The SEED allowed us to identify only two additional representatives of the NadE* branch beyond the seven strains of *F. tularensis*. As can be seen from the simplified tree (SI Fig. 8) of single-domain members of the NadE family in bacteria (same as those included in the NAD subsystem in SI Table 1 and in the multiple alignment in SI Fig. 7), a relatively well-separated NadE* branch contains the proteins from two species of the Pasteurellaceae group, *Mannheimia succinoproducens* and *Actinobacillus succinogenes.* Amino-acid sequences of both Pasteurellaceae enzymes are generally close to the sequence of *ft*NadE* (54% identity) and share with it a number of residues listed above as part of an NMN synthetase signature contributing to its unique substrate preference.

Colocalization of *M. succinoproducens* and *A. succinogenes nadE** genes in the same operon with the *pncB* gene encoding nicotinate phosphoribosyltransferase suggests that together these two enzymes may compose a new variant of the nicotinic acid (Na) salvage pathway (SI Fig. 2). In this pathway, Na would be transformed to NaMN by the PncB enzyme, followed by the amidation of NaMN to NMN intermediate, which would then be converted to the NAD cofactor by the NMN adenylyltransferase of the NadR family. The latter enzyme was previously characterized as the only housekeeping adenylyltransferase in *H. influenzae* (9). The NMN adenylyltransferase and the RNm kinase (encoded in the C-terminal domain of the NadR protein) activities together with the PnuC transporter compose the RNm salvage pathway that is present in all Pasteurellaceae, including *M. succinoproducens* and *A. succinogenes*. However, the presence of *pncB* and *nadE* homologs is the unique feature of the latter two strains. Identification of a similarly organized *pncB-nadE* operon in some Gram-positive bacteria suggests a possible evolutionary scenario that involves its horizontal transfer to a common ancestor of *M. succinoproducens* and *A. succinogenes*. As most of NAD biosynthetic machinery (including the NaMN adenylyltransferase of

NadD family) was lost in the common ancestor of all Pasteurellaceae, the NAD synthetase activity of the acquired conventional NadE enzyme would not give any competitive advantage. It is tempting to speculate that a fully functional NMN synthetase could have evolved in this genetic background starting from a low side-activity of the acquired (and otherwise obsolete) NAD synthetase enzyme. It is conceivable that an evolved *nadE** gene could become a subject of further horizontal transfer events, e.g., to an ancestor of *F. tularensis*. A combination of NMN synthetase with NMN adenylyltransferase (of the NadM family) would enable an alternative NAD biosynthetic route and allow the elimination of the functionally redundant conventional pathway from *F. tularensis*. Although the proposed evolutionary scenario is highly speculative, it allows us to explain most of the presently available data.

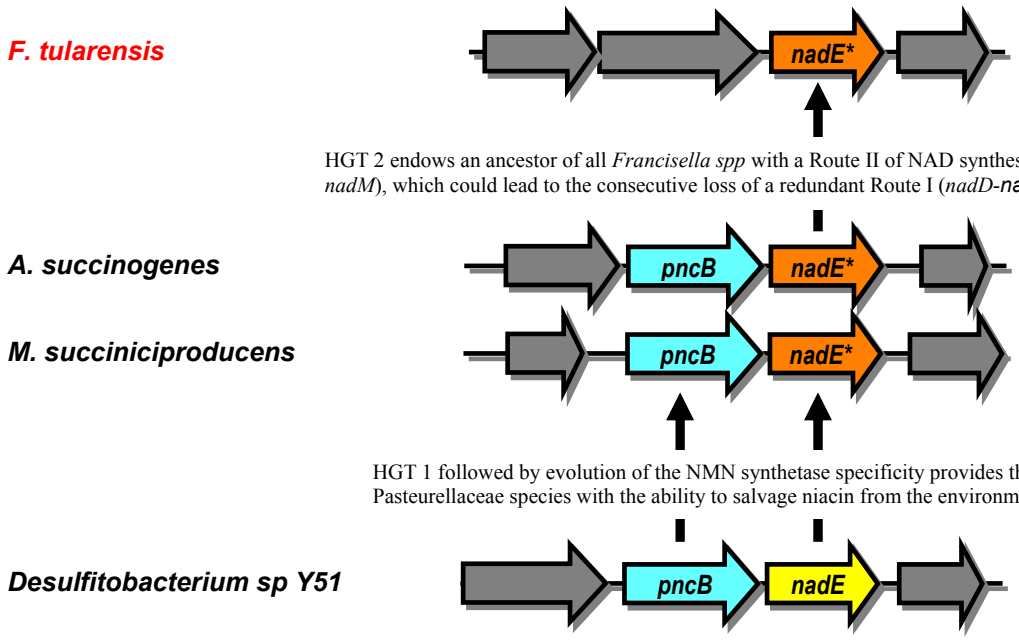

Comparison of the chromosomal arrangement of the *nadE and *nadE* genes.** In both members of Pasteurellaceae group, the gene *nadE** occurs in the operon-like chromosomal cluster containing gene *pncB*. A similar chromosomal arrangement can be found for the canonical *nadE* gene in a number of Gram-positive bacteria, as illustrated here for *Desulfitobacterium sp Y51*. Both genes, *pncB* and *nadE* from the latter organism, are close homologs of *pncB* and *nadE** genes from Pasteurellaceae (~43% and 48% identity, respectively). Genes surrounding this cluster and not conserved between any of these species are colored grey.

References

1. Osterman A, Grishin NV, Kinch LN, & Phillips MA (1994) Formation of functional cross-species heterodimers of ornithine decarboxylase. *Biochemistry* 33(46):13662-13667.
2. Daugherty M, Vonstein V, Overbeek R, & Osterman A (2001) Archaeal shikimate kinase, a new member of the GHMP-kinase family. *J Bacteriol* 183(1):292-300.
3. Otwinowski Z, Minor, W. (1997) Processing of X-ray diffraction data collected in oscillation mode. *Methods Enzymol.* 276:307-326.
4. Vagin A, Teplyakov, A. (1997) MOLREP: an automated program for molecular replacement. *J. Appl. Cryst.* 30:1022-1025.
5. Symersky J, Devedjiev Y, Moore K, Brouillette C, & DeLucas L (2002) NH3-dependent NAD+ synthetase from Bacillus subtilis at 1 A resolution. *Acta Crystallogr D Biol Crystallogr* 58:1138-1146.
6. Murshudov GN, Vagin AA, & Dodson EJ (1997) Refinement of macromolecular structures by the maximum-likelihood method. *Acta Crystallogr D Biol Crystallogr* 53:240-255.
7. Collaborative Computational Project N (1994) The CCP4 suite: programs for protein crystallography. *Acta Crystallogr D Biol Crystallogr* 50:760-763.
8. Emsley P & Cowtan K (2004) Coot: model-building tools for molecular graphics. *Acta Crystallogr D Biol Crystallogr* 60:2126-2132.
9. Kurnasov OV*, et al.* (2002) Ribosylnicotinamide Kinase Domain of NadR Protein: Identification and Implications in NAD Biosynthesis. *J Bacteriol* 184(24):6906-6917.
10. Gerdes SY*, et al.* (2006) Comparative genomics of NAD biosynthesis in cyanobacteria. *J Bacteriol* 188(8):3012-3023.
11. Segel IH ed (1993) *Enzyme Kinetics: Behavior and Analysis of Rapid Equilibrium and Steady-State Enzyme Systems* (John Wiley & Sons, Inc., New York).
12. Bisswanger H (2002) Enzyme Kinetics: Principles and Methods. ed Bubenheim L (Darmstadt:Wiley-VCH).
13. Gallagher LA*, et al.* (2007) A comprehensive transposon mutant library of Francisella novicida, a bioweapon surrogate. *Proc Natl Acad Sci U S A* 104(3):1009-1014.
14. Zogaj X, S. Chakraborty, J. Liu, D. Thanassi, K. Klose (2008) Characterization of the Francisella tularensis subsp. novicida type IV pilus. *Microbiology* 154.
15. Chamberlain RE (1965) Evaluation of Live Tularemia Vaccine Prepared in a Chemically Defined Medium. *Appl Microbiol* 13:232-235.
16. Baron GS, Myltseva SV, & Nano FE (1995) Electroporation of Francisella tularensis. *Methods Mol Biol* 47:149-154.
17. Maharjan RP & Ferenci T (2003) Global metabolite analysis: the influence of extraction methodology on metabolome profiles of Escherichia coli. *Anal Biochem* 313(1):145-154.

18. Bieganowski P, Pace HC, & Brenner C (2003) Eukaryotic NAD+ synthetase Qns1 contains an essential, obligate intramolecular thiol glutamine amidotransferase domain related to nitrilase. *J Biol Chem* 278(35):33049-33055.
19. Bellinzoni M*, et al.* (2005) Glutamine amidotransferase activity of NAD+ synthetase from Mycobacterium tuberculosis depends on an amino-terminal nitrilase domain. *Res Microbiol* 156(2):173-177.
20. Chaudhuri RR*, et al.* (2007) Genome sequencing shows that European isolates of Francisella tularensis subspecies tularensis are almost identical to US laboratory strain Schu S4. *PLoS ONE* 2(4):e352.
21. Petrosino JF*, et al.* (2006) Chromosome rearrangement and diversification of Francisella tularensis revealed by the type B (OSU18) genome sequence. *J Bacteriol* 188(19):6977-6985.
22. Larsson P*, et al.* (2005) The complete genome sequence of Francisella tularensis, the causative agent of tularemia. *Nat Genet* 37(2):153-159.
23. Rohmer L*, et al.* (2007) Comparison of Francisella tularensis genomes reveals evolutionary events associated with the emergence of human pathogenic strains. *Genome Biol* 8(6):R102.
24. Beckstrom-Sternberg SM*, et al.* (2007) Complete genomic characterization of a pathogenic A.II strain of Francisella tularensis subspecies tularensis. *PLoS ONE* 2(9):e947.
25. Edgar RC (2004) MUSCLE: multiple sequence alignment with high accuracy and high throughput. *Nucleic Acids Res* 32(5):1792-1797.
26. Clamp M, Cuff J, Searle SM, & Barton GJ (2004) The Jalview Java alignment editor. *Bioinformatics* 20(3):426-427.
27. Thompson JD, Gibson TJ, Plewniak F, Jeanmougin F, & Higgins DG (1997) The CLUSTAL_X windows interface: flexible strategies for multiple sequence alignment aided by quality analysis tools. *Nucleic Acids Res* 25(24):4876-4882.